KfK 4930
September 1991

Cryo-cooled High-power Window for High-frequency Plasma Heating

Thermodynamic Study of the Single-disk Concept with Liquid Nitrogen Edge Cooling

P. Norajitra, E. Bojarsky, H. Reiser, H.-E. Häfner
Institut für Materialforschung
Projekt Kernfusion

Kernforschungszentrum Karlsruhe

Kernforschungszentrum Karlsruhe

Institut für Materialforschung
Projekt Kernfusion

KfK 4930

Cryo-cooled High-power Window for High-frequency Plasma Heating

Thermodynamic Study of the Single-disk Concept with Liquid Nitrogen Edge Cooling

P. Norajitra, E. Bojarsky, H. Reiser, H. -E. Häfner

Kernforschungszentrum Karlsruhe GmbH, Karlsruhe

Als Manuskript vervielfältigt
Für diesen Bericht behalten wir uns alle Rechte vor

Kernforschungszentrum Karlsruhe GmbH
Postfach 3640, 7500 Karlsruhe 1

ISSN 0303-4003

Abstract:

Within the framework of gyrotron window development, IMF pursues the concept of a single-disk window with edge cooling. Compared to a double-disk window with surface cooling, this concept offers a number of advantages in terms of safety, reliability, and ease of design and fabrication. The coolants which can be used for this purpose are liquid nitrogen and helium at very low temperature.

The report deals with thermodynamic calculations of edge cooling with liquid nitrogen. The impacts on the performance limits of various parameters and factors are demonstrated.

Zusammenfassung:

Kryogen-gekühltes Hochleistungsfenster für Hochfrequenz-Plasmaheizung

Thermodynamische Untersuchung zum Einscheibenkonzept mit Flüssigstickstoff-Randkühlung

Im Rahmen der Gyrotronfensterentwicklung wird vom IMF das Konzept eines Einscheiben-Fensters mit Randkühlung verfolgt. Dieses Konzept bietet gegenüber dem Doppelscheibenfenster mit Flächenkühlung mehrere Vorteile in den Punkten Sicherheit, Zuverlässigkeit und einfache Bauweise. Als Kühlmittel kommen flüssiger Stickstoff und Helium bei sehr niedriger Temperatur in Betracht.

Im vorliegenden Bericht werden thermodynamische Rechnungen zur Randkühlung mit flüssigem Stickstoff behandelt. Es werden Auswirkungen von verschiedenen Parametern und Faktoren auf die Leistungsgrenze gezeigt.

Contents:

		pages:
1	Introduction	1
2	Design and Geometry of the Single-disk Window	2
3	Problem	3
4	Power Absorption in the Window	3
	4.1 Gaussian Power Distribution Function	3
	4.2 Power Density in the Resonant Window	4
5	Materials Data	5
	5.1 Loss Tangent	5
	5.2 Dielectric Constant, ε_r'	6
	5.3 Thermal Conductivity	6
6	Calculation	7
	6.1 Method of Calculation	7
	6.2 Boundary Conditions and Conditions of Heat Removal	7
	6.2.1 Convective Boiling	8
	6.2.2 Nucleate Boiling	9
	6.2.3 Critical Heat Flux Density	10
	6.3 Verifying the Convergence Condition	11
	6.4 Reference Data	12

7 Result 13

7.1 Reference Case 13

7.2 Variation of Geometry 14

7.2.1 The Window Thickness, s 14

7.2.2 The Disk Diameter, D 14

7.2.3 The Thickness of the Window Edge, h 15

7.2.4 The Waveguide Diameter, D_W 15

7.2.5 Optimization of the Adiabatic Zone 16

7.3 The Influence of the Coolant Temperature, T_C 16

7.4 The tan δ Uncertainty 17

7.5 General Description of the Performance Limit 17

8 Transient Analysis 19

9 References 21

1 Introduction

As part of the development of high-frequency heating systems for fusion plasmas, the Karlsruhe Nuclear Research Center performs work on microwave power generation in gyrotrons. Window systems are required both as vacuumtight closure of the gyrotron relative to the transmission system and upstream of the feed point into the fusion plasma. The goal of this development work is a 1 MW high-power window for permanent operation.

The concept pursued is that of a single-pane window with edge cooling. Compared to double-disk windows with surface cooling, this concept offers the advantage of there being no coolant in the area of the high-frequency beam. This makes for complete freedom in the type of cooling adopted for the edge of the window and, should a window break, coolant would not necessarily penetrate into the gyrotron and/or the transmission system. Moreover, the single-disk design promises to be simpler and more reliable. Benefits are such that the drawback, i.e. less effective heat removal through the edge of the window, compared to surface cooling in the double disk, can be put up with.

To achieve this development goal, a window material of high thermal conductivity and low power absorption is required. Sapphire is the favorite material of choice. This Al_2O_3 single crystal has all these favorable properties at low temperatures. Cooling with liquid nitrogen and also with helium at very low temperature is being envisaged.

This study deals with the liquid nitrogen cooling principle adopted as the first step. It is less expensive technically and also more economic in operation. The effects on the performance limits of various parameters and factors are indicated, and the uncertainties still existing are shown.

The next study will deal with helium cooling.

2 Design and Geometry of the Single-disk Window

Figure 1 shows the design principle of the single-disk window with edge cooling in a vertical arrangement.

The window, which is a sapphire disk of 140 mm diameter and approx. 3.5 mm thickness, is fitted gastight into the waveguide. The required window thickness in the waveguide can be achieved by grinding the sapphire disk in a plane parallel way. The sapphire disk will be attached to the waveguide by means of metal collars made of FERNICO (iron-nickel-cobalt) material.The parts will be soldered together. Additional metalization of the surfaces of the cooled edge is required to improve heat transfer. In the simplest case, the energy absorbed in the window is removed by nucleate boiling at the edge of the disk in an annulus filled with liquid nitrogen at atmospheric pressure. It must be ensured that the LN_2 volume to be evaporated is supplied reliably and the relatively large vapor volumes produced can be dissipated freely. The parameters used in the calculation are shown in Fig. 2. They are defined as follows:

P_G [W]	gyrotron power transmitted
Q_R [W]	thermal power dissipated radially
s [m]	resonant window thickness
D_O [m]	sapphire disk diameter
h [m]	thickness of window edge
D_W [m]	waveguide diameter
t [m]	wall thickness of waveguide
D_{A_o} [m]	outer diameter of collar support
D_{A_i} [m]	inner diameter of collar support
b [m]	wall thickness of attachment collar
T_C [K]	temperature of liquid nitrogen coolant
α [W/m^{2}K]	heat transfer coefficient
r [m]	window radius

3 Problem

The single-disk concept with edge cooling by liquid nitrogen incorporates two decisive problems: The radial heat removal from the central, energy absorbing, zone to the edge zone, and reliable cooling of the edge of the disk by nucleate boiling or pool boiling, respectively, without a transition to film boiling. In the first problem, the size and distribution of the heat source density, which is influenced directly by the loss tangent, and thermal conductivity play the most important roles. However, also the window thickness, edge thickness, and waveguide diameter are factors of interest in the optimization of a single-disk window. The boundary condition is reached in each case as soon as stable operation is exceeded and temperatures rise exponentially.

All these parameters will be treated below on the basis of pool boiling of the nitrogen assumed to arise at 1 bar and 0.4 bar coolant pressure. The cooling effect during boiling, and its limits, are investigated experimentally along with this theoretical study.

4 Power Absorption in the Window

4.1 Gaussian Power Distribution Function

The radial distribution of gyrotron power density in the window can be described by this relation:

$$p(r) = P_G \cdot f_z(r) \qquad [W/m^2] \qquad (1)$$

with P_G [W] as the impinging gyrotron power,

and $f_z(r)$ [1/m²] as the distribution function.

For the HE_{11} mode studied at KfK, $f_z(r)$ can be written as a Gaussian distribution, neglecting minor scattering components in the r- and ϕ-directions [1]:

$$f_z(r) = \frac{1.1003}{R_W^2} \cdot e^{\frac{-1}{0.3} \cdot (r/R_W)^2} \quad [1/m^2] \qquad (2)$$

with R_W [m] = $D_W/2$, the waveguide radius, and r [m], the window radius.

This function is plotted in Fig. 3 for $R_W = 44.45 \cdot 10^{-3}$m.

4.2 Power Density in the Resonant Window

The power fraction absorbed in the window material is calculated from this relation [2]:

$$q_V(r) = p(r) \cdot 2\pi \frac{f}{c} \cdot \sqrt{\varepsilon_r'} \cdot \tan\delta \cdot S \quad [W/m^3] \qquad (3)$$

with $S = (1 + \varepsilon_r')/2\sqrt{\varepsilon_r'}$ (4)

where f [1/s] is the wave frequency, c [m/s] the velocity of light in the vacuum, ε_r' [-] the dielectric constant, tan δ [-] the loss tangent, and S [-] the anti-resonance factor.

This relation applies to a tuned resonance thickness of the window, which is determined as follows:

$$s = \frac{N_\lambda \cdot c}{2f \cdot \sqrt{\varepsilon_r'}} \quad [m] \qquad (5)$$

where N_λ is the number of half wavelengths. Table 1 lists the resonance thicknesses for N_λ between 1 and 10 on the basis of an average temperature of 100 K. According to [2], the error of s may be up to approx. 0.04 mm.

5 Materials Data

5.1 Loss Tangent

The main factor responsible for energy absorption in the window material is the so-called loss tangent (tan δ). Because of its quadratic dependence on temperature, this quantity is particularly important in thermodynamic considerations.

According to [3], an average temperature relation of tan δ for unirradiated sapphire in the temperature range between 95 K and 330 K is :

$$\tan \delta = 1.5 \cdot 10^{-9} \cdot T^{2.07} \qquad (6)$$

with T, the temperature, in [K].

For the following calculation, tan δ values for lower temperatures down to 70 K are simply extrapolated.

Figure 4 shows the average development of tan δ (curve b) for a temperature range between 70 K and 140 K.

In line with the measurement error range indicated, the upper and the lower bounds of the measured values for this temperature range can be indicated as follows:

Upper bound (curve a):

$$\tan \delta_{max} = 2.3 \cdot 10^{-9} \cdot T^{2.07} \qquad (7)$$

Lower bound (curve c):

$$\tan \delta_{min} = 0.7 \cdot 10^{-9} \cdot T^{2.07} \qquad (8)$$

5.2 Dielectric Constant, ε_r'

The temperature dependent relation of ε_r' for sapphire is taken from [3] and reads as follows:

$$\varepsilon_r' = 9.405 + 0.0005 \cdot (T-300) \qquad (9)$$

with T, the temperature, in [K].

The corresponding curve is shown in Fig. 5.

5.3 Thermal Conductivity

Figure 6 shows a plot of the thermal conductivity of sapphire as a function of temperature. The data were taken from [4]. For a temperature range between 70 K and 140 K, they are between 1500 and 170 W/mK.

For the collar material, FERNICO, the data for stainless steel as taken from [5] were employed. They are listed in Table 2.

6 Calculation

6.1 Method of Calculation

The Fourier differential equation of thermal conduction is solved in the following way:

$$q(T) = -\lambda(T) \cdot \text{grad}\, T \qquad (10)$$

with the heat flux density, q, and thermal conductivity, λ, themselves being a function of the temperature variable, T (see Sections 4.2 and 5). This clearly shows the non-linearity of the differential equation.

The ABAQUS finite-element program [6] is used for the numerical solution of this problem. Figure 7 shows the rotationally symmetrical finite-element model of the sapphire disk in the r,z-plane. For reasons of symmetry, only half a disk thickness is considered. The disk is subdivided into three radial zones, namely the inner zone with the heat input, the intermediate zone between the waveguide and the collar support, and the cooled edge zone from the collar support to the edge of the disk. The zone in between is conservatively assumed to be an adiabatic zone, which means that it does not transmit any heat to the outside.

6.2 Boundary Conditions and Conditions of Heat Removal

Convective heat transfer follows this general setup:

$$q = \alpha \cdot \Delta T = \alpha \cdot (T_W - T_C) \qquad [W/m^2] \qquad (11)$$

with

q [W/m²] as the surface heat flux density,

α [W/m²K] as the heat transfer coefficient, and

ΔT [K] as the temperature difference between the wall and the coolant.

Heat is removed by nitrogen boiling in the free convection mode. The preferred coolant pressure in this case is 1 bar. However, it is also possible to set a lower boiling pressure and , in this way, lower the boiling temperature. This requires a certain amount of technical expense in order to ensure stable operation.

Heat transfers in the convective boiling and nucleate boiling regimes and the transition from nucleate boiling to film boiling (critical heat flux density) are estimated. Essentially, the data and relations indicated in the VDI-Wärmeatlas [7] are used.

6.2.1 Convective Boiling

Convective boiling without bubble formation plays a role only at very low heat flux densities on the heating surface. Calculation follows this relation:

$$Nu = \frac{\alpha \cdot L}{\lambda} = 0.15 \cdot (Gr.Pr)^{1/3} \qquad (12)$$

$$with \;\; Gr = \frac{L^3 g \beta}{\nu^2} (T_W - T_{fl}) \qquad (13)$$

where β [1/K] is the expansion coefficient, ν [m^2/s] the kinematic viscosity, T_W [K] the surface temperature of the window edge, T_{fl} [K] the boiling temperature of nitrogen according to [8].

The outside diameter, D_O, of the window was substituted for the length, L. At an operating pressure of 1 bar, the transition from convective boiling to nucleate boiling occurs at a heat flux density of $q < 700$ W/m² (Fig. 8). This means that convective boiling is of no practical significance when the window is cooled with liquid nitrogen.

6.2.2 Nucleate Boiling

To determine the heat transfer coefficient, α, in the case of nucleate boiling, empirical and semi-empirical setups are used in [7] which are based on the results of systematic test series. A normalized heat transfer coefficient, α/α_o, is used with this setup:

$$\frac{\alpha}{\alpha_o} = F(p^*) \cdot \left[\frac{q}{q_o}\right]^{n(p^*)} \cdot \left[\frac{R_p}{R_{po}}\right]^{0.133} \qquad (14)$$

This takes into account the following parameters:

- **Operating pressure, p [bar]**

  in the form of $p^* = p/p_c$ (p_c = critical pressure). For nitrogen, the setup is:

$$F(p^*) = 1.2 \cdot p^{*0.27} + \left(2.5 + \frac{1}{1-p^*}\right) \cdot p^* \qquad (15)$$

In this case, the p_o^*normalization value is 0.1, which assigns the value of 1 to $F(p_o^*)$. The critical pressure for nitrogen is 34.0 bar. By way of example, the following relations hold:

Operating pressure, p [bar]	1.0	0.75	0.4	0.2
Boiling temperature, T_s [K]	77.35	75	70	65
Normalized pressure, p* [-]	0.0294	0.0206	0.0118	0.0059
F(p*)	0.567	0.506	0.403	0.321

- **Heat flux density, q [W/m²]**

In the experiments quoted in [7], the normalization value was q_o = 20,000 W/m². The exponent n in Equation (14) determined in that case obeys this relation for nitrogen:

$$n = 0.9 - 0.3 \cdot (p^*)^{0.3} \qquad (16)$$

- **Roughness of the heating surface, R_p [m]**

The normalization value of roughness was R_{po} = 1 µm in all experiments. Potential improvements of heat removal as a result of roughness should be left out of account in this assessment (R_p/R_{po} = 1).

The heat transfer coefficient, α_o, in relation (14) in the normalization values referred to above was measured mainly in horizontal pipes made of copper. For nitrogen, the value found was α_o = 10,000 W/m²K. In a first approximation, this value should apply also to heat transfer at the edge of the window made of sapphire, as this is metallized.

Consequently, the relation for the heat transfer coefficient in the case of nucleate boiling is

$$\alpha = 10^4 \left(\frac{q}{20000} \right)^{n(p)} \cdot \quad F(p) \qquad (17)$$

This is plotted in Fig. 8 as a function of q for some operating pressures of interest.

6.2.3 Critical Heat Flux Density

The maximum heat flux density, q_{krit} (transition from nucleate boiling to film boiling) has this setup in [7]:

$$q_{krit} = k_1 \cdot \quad \Delta h_v \cdot \quad \rho_g^{0.5} \cdot \quad (\sigma \cdot \quad (\rho_l - \rho_g) \cdot \quad g)^{0.25} \qquad (18)$$

with Δh_v heat of evaporation,

ρ_l, ρ_g densities of the liquid and the vapor,

σ surface tension.

If the relation

$\sigma \sim (\rho_l - \rho_g)^4$

is taken into account, Equation (18) becomes

$$q_{krit} = k_1 \cdot \Delta h_v \cdot \rho_g^{0.5} (\rho_l - \rho_g)^{1.25} \qquad (19)$$

The factor k_1 in relation (19) is indicated to be 0.13 to 0.16.

Substituting the constitutional data from [8] and k_1 = 0.13 furnishes as the maximum heat flux densities (see also Fig. 8):

Operating pressure, p [bar]	1	0.75	0.4	0.2
$q_{krit} \cdot 10^4$ [W/m²]	23.7	21.7	17.1	13.2

6.3 Verifying the Convergence Condition

The actual computation run is preceded by a number of systematic trial runs in which the impacts of the non-linearity of the problem upon the convergence behavior of the program can be recognized. In ABAQUS, the TEMTOL quantity is used as a yardstick for checking convergence. In the study, both the calculated center temperature of the window and the balance of thermal power supplied and extracted are observed.

In a first step, an example taken from [9] of an analytical solution dealing with thermal conduction in a round bar with internal heat sources is used. Accordingly, for a round bar with the radius R [m], at a constant heat source density, q_V [W/m³], and a constant thermal conductivity, λ [W/mK], the temperature difference, ΔT [K], between the center and the edge is this:

$$\Delta T = \frac{q_V \cdot R^2}{4\lambda} \quad [K] \qquad (20)$$

In a trial run with ABAQUS, constant values for q_V, λ, and for the heat transfer coefficient, α, are substituted. Even at a required TEMTOL of 10^{-2}, the result is already completely identical to the exact solution. The balance of powers is observed precisely.

In the next step, the complete model with all temperature dependent quantities is used. It is seen that, if all complex dependency relations are taken into account, TEMTOL must be $\leqq 10^{-6}$. Only then will it be possible to guarantee that the balance of powers and, consequently, the stability of the temperature field is observed.

6.4 Reference Data

As a starting position for other parametric calculations, the following reference data are defined as listed below:

s = 1.756 mm

D_O = 140 mm dia.

h = 3.5 mm

D_W = 88.9 mm dia.

t = 3.5 mm

D_{A_O} = 114 mm dia.

D_{A_I} = 104 mm dia.

b = 0.6 mm

T_C = 77.35 mm

Mean tan δ-values (Curve b, Fig. 4).

7 Result

7.1 Reference Case

Figures 9 to 13 show the results for the reference case (Item 6.4).

Figure 9 indicates the radial temperature distribution in the window as a function of the gyrotron power. A rapid rise in the window center temperature, T_o, and in the thermal power, Q_R, is observed as the gyrotron power rises. The development of T_o and Q_R versus the gyrotron power is shown in Fig. 10. Stable window operation can be seen up to a gyrotron power of approx. 0.3 MW. This is followed by a range in which levels increase exponentially up to the point of thermal runaway. The gyrotron power limit at which runaway starts is defined by P_G^{max}. In this case, it is 0.33 MW. The radial distributions of tan δ (Eq. 6) and q_V (Eq. 3) resultant at P_G^{max} are shown in Fig. 11. It is easy to see a characteristic Gaussian distribution in accordance with Fig. 3. In the center of the window, the maximum value of q_V is 100 W/cm^3. The integral value of the absorbed thermal power, Q_R, is plotted versus the window radius in Fig. 12. The cumulated total is 216 W. The second curve in this diagram shows the radial heat flux density, q_R, which is taken as a measure of the temperature gradient (Eq. 10). The curve attains a peak of approx. 61 W/cm^2 at a radius, r, of approx. 22 mm.

Figure 13 shows the corresponding heat removal conditions for the cooling zone (r = 52-70 mm). This zone is made up of two regions: the first region with the collar support (r = 52-57 mm), and the second region with the free sapphire surface (r = 57-70 mm). The diagram shows the curves of q and α pertaining to the respective cooling surface. Because of the relatively poor thermal conductivity of FERNICO, the value of q on the collar surface averages only 1.4 W/cm^2. Immediately behind the collar support, the peak value of q is around 3 W/cm^2, which is still far below the critical value. Then values of q decrease exponentially to some 1 W/cm^2 at the edge of the disk.

In accordance with the relation in Eq. 17, a similar development is found for α. The maximum value of α is 0.75 W/cm^{2}K. The result shows that the runaway point is determined not by a critical state in the cooling zone, but by the maximum removable thermal power from inside the window. This behavior is generally referred to as the "bottleneck effect."

7.2 Variation of Geometry

7.2.1 The Window Thickness, s

On the basis of the reference assumptions made under Item 6.4, Fig. 14 shows the radial temperature distribution in the window for various window thicknesses. The gyrotron power is kept constant at 0.3 MW. A slight exponential increase in the center temperature of the window is observed as the thickness of the window increases. This can be explained by this feedback effect: As the window thickness increases, more thermal power is absorbed which, automatically, results in a higher ΔT in the cooling zone and also in a rise in the temperature gradient towards the center of the window. This, in turn, raises the tan δ values, thus causing even higher thermal absorption.

7.2.2 The Disk Diameter, D_O

This section is devoted to studies of the influence on window temperature exerted by the diameter of the sapphire disk. The calculations are run for D_O = 140, 130, 120, and 114 mm under the other reference conditions listed under Item 6.4 and at P_G = 0.3 MW.

Figure 15 shows the respective temperature distributions for the disk diameters listed above. Reducing the disk diameter from 140 to 130 mm is seen to result in only a slight increase in the center temperature. This can be explained by the relatively low heat flux density, q, with a flat curve prevailing in this outer zone (see Fig. 13).

Further decreasing D_O leads into a steeper region of q, which raises ΔT in the cooling zone. As a result of the temperature feedback to the inside of the window, the center temperature is increased considerably.

7.2.3 The Thickness of the Window Edge, h

Changes in the thickness of the window edge, h, primarily influence the temperature gradient in the adiabatic transition zone and, consequently, also the center temperature of the window.

Figure 16 shows the temperature distribution in the window for h = 3.5, 5, 7, and 10 mm at P_G = 0.3 MW. The resultant center temperatures are plotted versus the thickness of the window edge in Fig. 17. The result shows the change in the center temperature to be most pronounced in the range of h = 3.5 - 5 mm.

7.2.4 The Waveguide Diameter, D_W

A given waveguide diameter, D_W, is used to define both the distribution function of the power density (Eq. 2) in the window and the edge cooling surface available.

A higher peak value of the power density is encountered with a smaller waveguide diameter and vice versa. At a constant disk diameter, the cooled surface in the edge zone can be widened by reducing the size of the waveguide.

Figure 18 shows the result of the variation of D_W between 60 and 115 mm at P_G = 0.3 MW. For the rest, the same conditions apply as in the reference case. The center temperatures determined in this way are plotted versus D_W in Fig. 19. Accordingly, the optimum is around $D_W \approx 103$ mm. The underlying waveguide diameter of 88.9 mm is still in a relatively favorable range.

7.2.5 Optimization of the Adiabatic Zone

Figure 20 shows an alternative draft of the collar design. The interesting feature of this design is the flatter shape of the collar with D_{A_O} = 108.6 mm and D_{A_I} = 98.6 mm, which achieves an 11% larger cooling surface and a 36% shorter adiabatic zone. Compared with the investigation under Item 7.2.2, the cooling surface achieved in this way would correspond to a fictitious disk diameter of 146 mm. However, the result has shown that, at $D_O > 140$ mm, only a slight improvement can be achieved. Consequently, mainly the influence of the design of the adiabatic zone is to be shown here. The reduced length for radial heat transfer referred

to above already would result in a slight decrease of the center temperature. Combination with an increase in the radial area in this zone (with h = 5 mm) results in a better runaway behavior than is shown in the reference case (Fig. 21). The runaway point in this case is at 0.35 MW.

7.3 The Influence of the Coolant Temperature, T_C

The coolant temperature, T_C, can be lowered by reducing the boiling pressure (table in 6.2.2). On the basis of the reference data in 6.4, Figures 22 to 24 show the results in case of a coolant temperature, T_C, of 70 K.

The lower temperature level has a beneficial effect both on the thermal power absorption (tan δ) and on the thermal conductivity of sapphire. In the cooled zone, the thermal conductivity is around 70% higher than in the reference case, which makes for a more uniform distribution on the cooled surface of the thermal power delivered there. Despite the lower heat transfer coefficient resulting from the lower boiling pressure, the overall result is still a gain. Compared with the results for T_C = 77.35 K (Figures 9-13), the runaway point is reached only at P_G^{max} = 0.449 MW. The maximum amount of thermal power to be dissipated, Q_R^{max}, at which the bottleneck effect occurs, amounts to 237 W. Because of the more favorable temperature and heat flux distributions, it is approx. 10% higher than in the reference case.

Figure 25 shows the temperature distributions in the window at coolant temperatures of 70, 72.5, 75, and 77.35 K and at a gyrotron power of 0.3 MW. In this case, the influence of the coolant temperature on power absorption and on the center temperature of the window is evident. At T_C = 77.35 K, the power absorbed is 43% higher than at T_C = 70 K.

7.4 The tan δ Uncertainty

The uncertainties of tan δ imply the large error band of the measured values. Moreover, no reliable data are as yet known for temperatures below 95 K.

For the study described below, the relations shown in Fig. 4 for maximum, medium and minimum values of tan δ are used as a basis.

Figure 26, for instance, shows the respective temperature distributions in the window at P_G = 0.2 MW under all the other reference conditions. A pronounced effect of the tan δ uncertainty is seen. While, in the most favorable case (minimum values of tan δ), window temperatures are still low, the most adverse case (maximum values of tan δ) implies a state very close to the runaway point, despite the relatively low gyrotron power.

Figures 27 and 28 show the results with the most favorable tan δ values. Thermal runaway in this case occurs not before 0.707 MW, which is roughly 2.1 times higher than in the reference case. With an optimistic combination with a lower coolant temperature of 70 K, the runaway point is reached even as far as slightly less than 1 MW gyrotron power (Fig. 29).

Figures 30 and 31 show the corresponding results for the pessimistic case with the maximum values of tan δ.

If the influence of the coolant temperature is left out of account, for the time being, the range of the limit power of the gyrotron, because of the tan δ uncertainty, ranges between 215 and 707 kW. The corresponding mean value of 461 kW is about 40% higher than the limit power determined in the reference case. This means that the assumed mean curve of tan δ is pessimistic in the reference case.

The result shows that the influence of tan δ dominates very strongly. The error limits of tan δ must be narrowed down by better measuring techniques to ensure that more precise statements can be made about the power limit.

7.5 General Description of the Performance Limit

Figure 32 shows the limit of gyrotron power, P_G^{max}, as a function of the window thickness, coolant temperature, and the degree of tan δ. A relatively weak dependence on window thickness can be seen. The value of P_G^{max} increases slightly as the window thickness decreases. The dependence becomes even stronger at low-

er coolant temperature and minimum values of tan δ. At a normal liquid nitrogen temperature of 77.35 K (solid curves), a theoretical range for P_G^{max} of 200-800 kW can be indicated.

Reducing the coolant temperature produces a higher gain in P_G^{max} , as is shown by the curves for T_C = 70 K. Accordingly, e. g., a P_G^{max} of up to 0.5 MW can be attained at a window thickness of 0.7 mm under the assumption of medium tan δ values.

The dominating influence of tan δ is evident in this diagram. A power limit of 1 MW can be achieved only under the most favorable conditions (minimum values of tan δ and T_C = 70K) at window thickness of 1.4 mm.

Figure 33 shows the development of the maximum thermal power which can be dissipated radially, plotted as a function of the window thickness and the coolant temperature. The curves apply to all assumptions of tan δ. With increasing window thickness, the specific maximum heat removal per unit thickness of the window is seen to decrease continuously. This, accordingly, leads to an earlier onset of runaway, as is seen from Fig. 32.

In summary, it is safe to say this:

- The runaway behavior and therewith the performance limit of the window is determined by the interplay of the strong temperature dependence of tan δ with the also unfovarable temperature dependence of the thermal conductivity of sapphire.
- Of all the parameters investigated, tan δ exerts the strongest influence. As a consequence of the large uncertainty associated with tan δ, it is not yet possible to indicate a precise power limit.
- The maximum temperature difference in the window between the center and the edge at runaway is around 50 K.
- The critical surface heat flux density in the cooled zone is not reached.

8 Transient Analysis

The development of temperature in the window as a function of time must be known if the window is to be subjected to short pulse loads at elevated transmission powers. In this section, conditions at P_G = 0.5 MW and t = 1 s are considered without interruption of the cooling. The reference data taken from 6.4 will be used also for this purpose.

Figure 34 shows the specific thermal capacity, c_p, of sapphire [4] and steel [5] as a function of temperature. The medium value for sapphire, e. g. at 115 K, is approx. 170 J/kg K. The value assumed for the collar, with T ≈ 80 K, is at 210 J/kg K. The density is assumed to be constant for sapphire at 3900 kg/m^3 and steel at 7970 kg/m^3.

Figure 35 shows the calculated development, as a function of time, of the window center temperature between 0 and 1.2 s for the case with P_G = 0.5 MW (top curve). For comparison, the corresponding curve is also plotted for the condition, as yet stable, with P_G = 0.33 MW (bottom curve) (see Item 7.1). The asymptotic shape of the bottom curve relative to a steady state is plain to see. On the other hand, the top curve shows a clear tendency of runaway already beginning at t = 1 s.

The maximum center temperature at the time t = 1 s is approx. 144 K. This corresponds to a maximum temperature differential, ΔT_{max}, in the window between the center and the edge of about 64 K. At a larger window thickness of 3.5 mm (Fig. 36) the corresponding center temperature attains a level of 155 K. This results in a ΔT_{max} of approx 75 K. Until the time considered of t = 1 s, there is no excessive effect as yet of the increased thickness of the window.

In the absence of strength data about sapphire in the low temperature range it is difficult to indicate the permissible limit of the temperature difference. In the literature, data even for steady-state loads at room temperature are quoted in a wide range of 100-150 K. At low temperature, the thermal linear expansion of sapphire is relatively slight, which implies that even higher limits are to be expected. It can be hoped, therefore, that the maximum temperature difference of 75 K determined in this way is still permissible for repeated thermal stresses. A more precise stability study will have to be conducted to corroborate this assumption.

Acknodledgements

This work has been performed in the framework of the Nuclear Fusion Projekt of the Kernforschungszentrum Karlsruhe.

9 References

[1] H.-U. Nickel,
February 1990, unpublished.

[2] J.-G. Wégrowe, F. Moons, M. Vassiliadis, E. Zolti,
Limits of Operation of Conventional RF Windows for Electron Cyclotron Wave Launchers in a Reactor,
NET-Report EURFU/XII-80/86/66, 1986.

[3] R. Heidinger,
Dielectric Loss of Alumina between 95 K and 330 K at ECRH Frequencies,
Journal of Nuclear Materials, vol. 173, pp. 243-246, 1990.

[4] Y.S. Touloukian et al.,
Thermophysical Properties of Matter,
vol. 2: Thermal Conductivity-Nonmetallic Solids,
vol.13: Thermal Expansion-Nonmetallic Solids,
IFI/Plenum, New York-Washington, 1970.

[5] Handbook on Materials for Superconducting Machinery,
National Bureau of Standards, Boulder, Colorado, January 1977.

[6] Hibbitt, Karlsson & Sorensen,
ABAQUS User's Manual, Version 4.8, 1989,
Providence, R.I., USA.

[7] VDI-Wärmeatlas,
Berechnungsblätter für den Wärmeübergang, Abschnitt Ha,
5th edition, 1988,
VDI-Verlag Düsseldorf.

[8] B. A. Hands,
NIPROP, A Computer Package for the Thermodynamic and Thermophysical Properties of Nitrogen,
Cryogenic Laboratory, Dept. of Engineering Science,
University of Oxford, Departmental Report No. 1485/83,
June 1983.

[9] M.A. Michejew,
Grundlagen der Wärmeübertragung, pp. 290 ff,
VEB-Verlag Technik, Berlin, 1964.

Table 1: Resonance thickness of the window ($\overline{T}$ = 100 K)

N_λ	s (mm)
1	0.351
2	0.702
3	1.054
4	1.405
5	1.756
6	2.107
7	2.459
8	2.810
9	3.161
10	3.512

Table 2: Thermal conductivity

Temperature (K)	λ(W/mK)	
	18/12 stainless steel [5]	Sapphire [4]
60	6.6	2650
70	7.5	1530
80	8.2	960
90	8.8	640
100	9.3	450
200	12.9	82

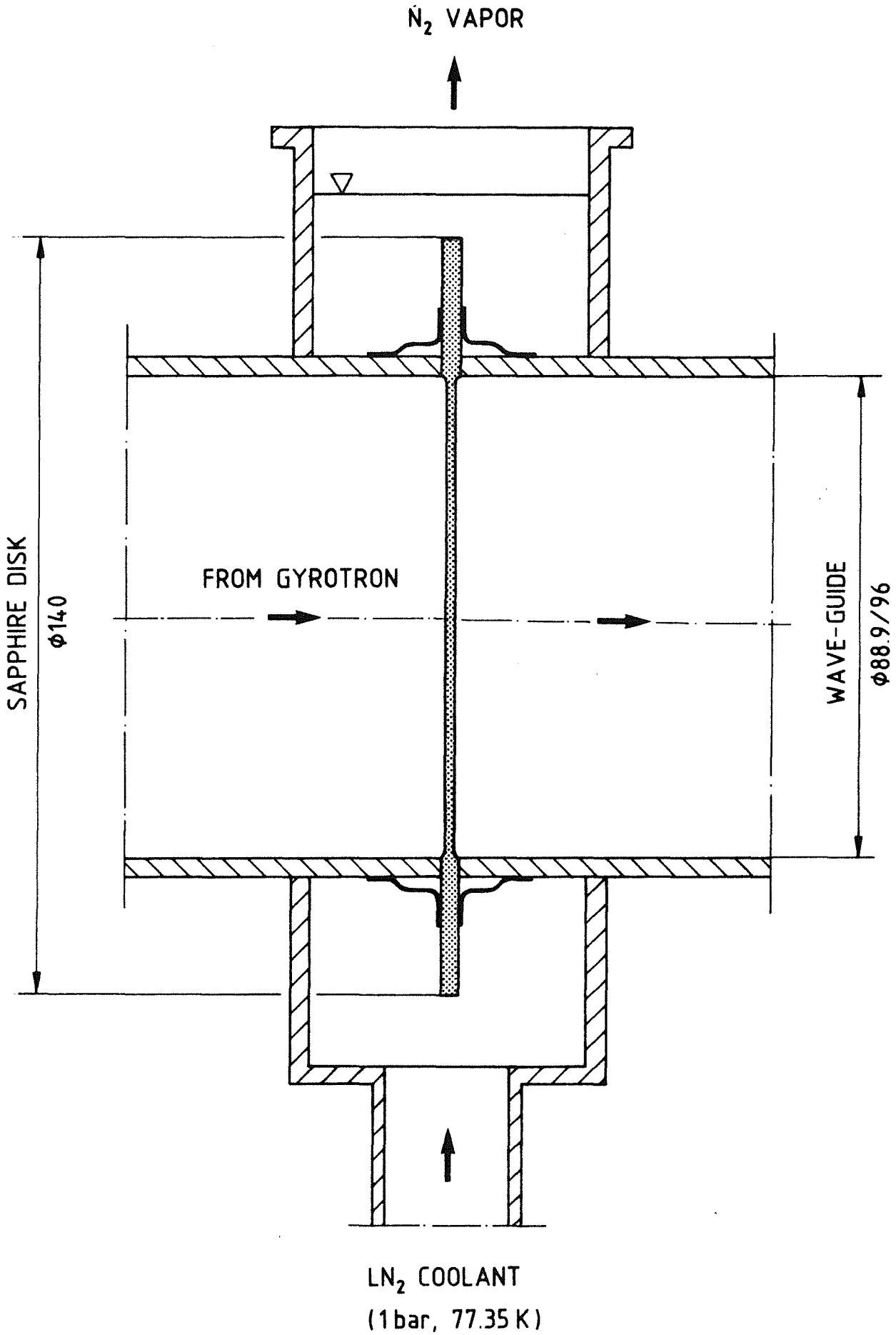

Fig. 1 Schematic design of the single-disk window with edge cooling in an open liquid-nitrogen bath

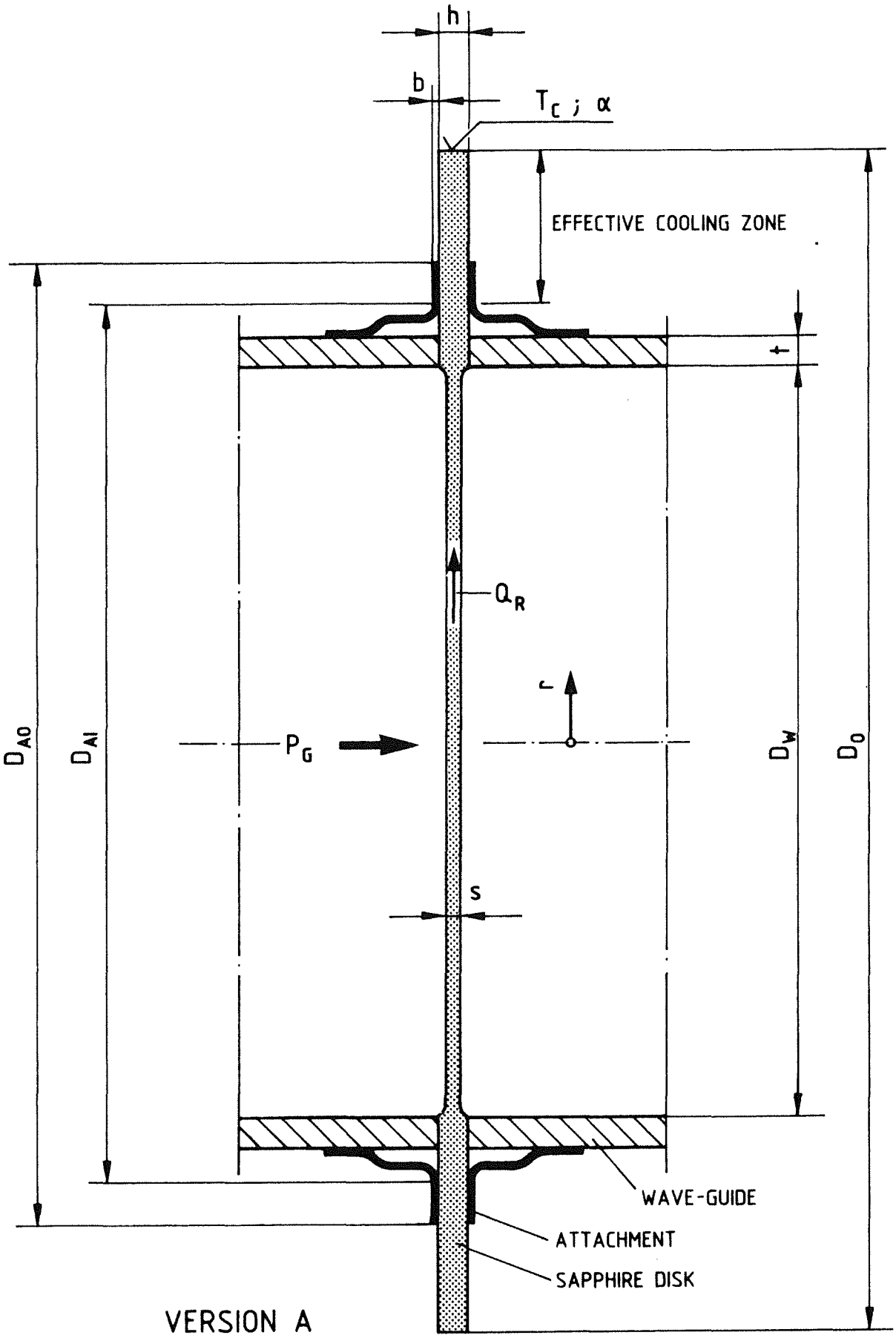

Fig. 2 Definition of the parameters for calculation

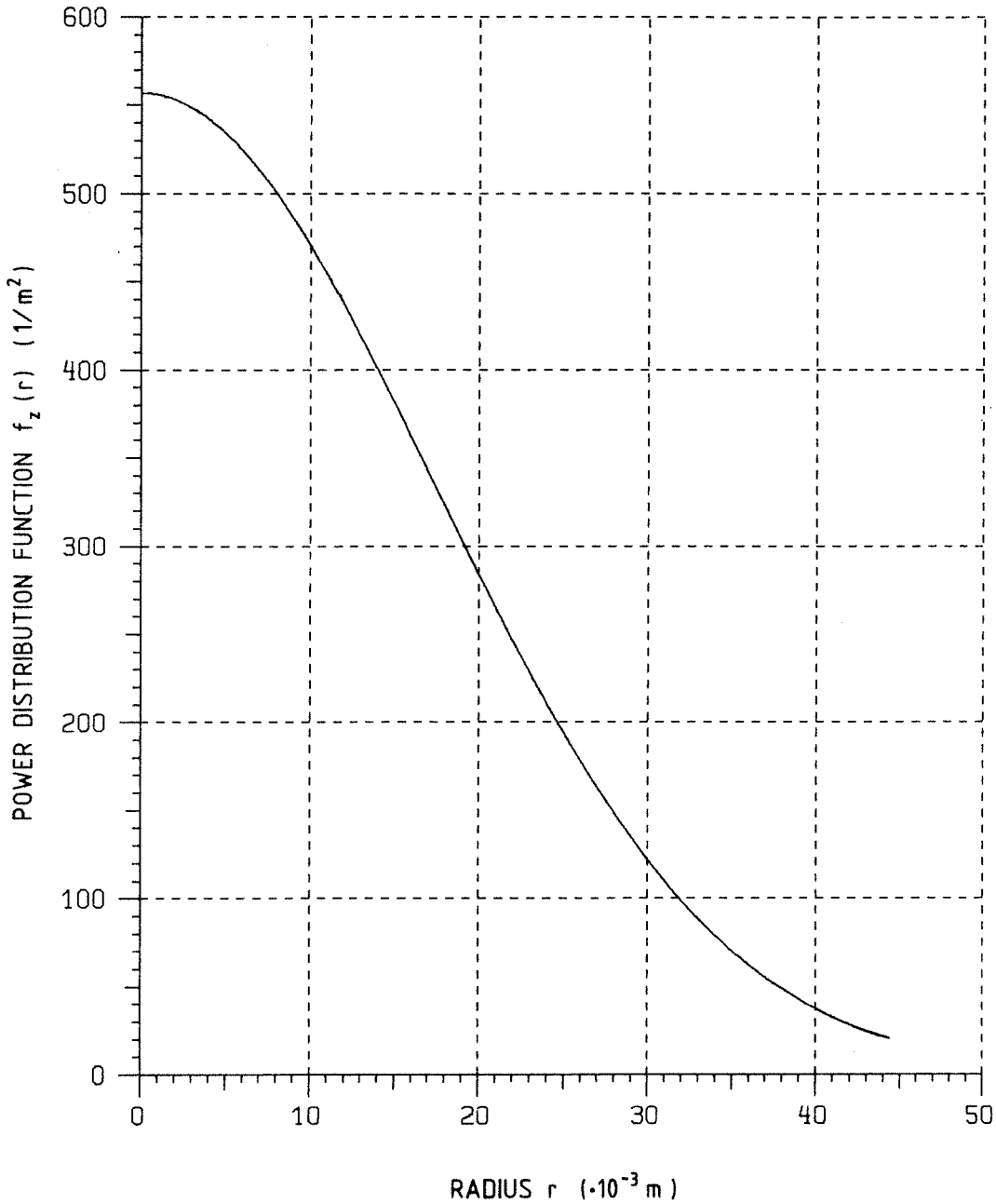

Fig. 3 Distribution function of the power density for the power transmitted according to the HE_{11} mode /1/

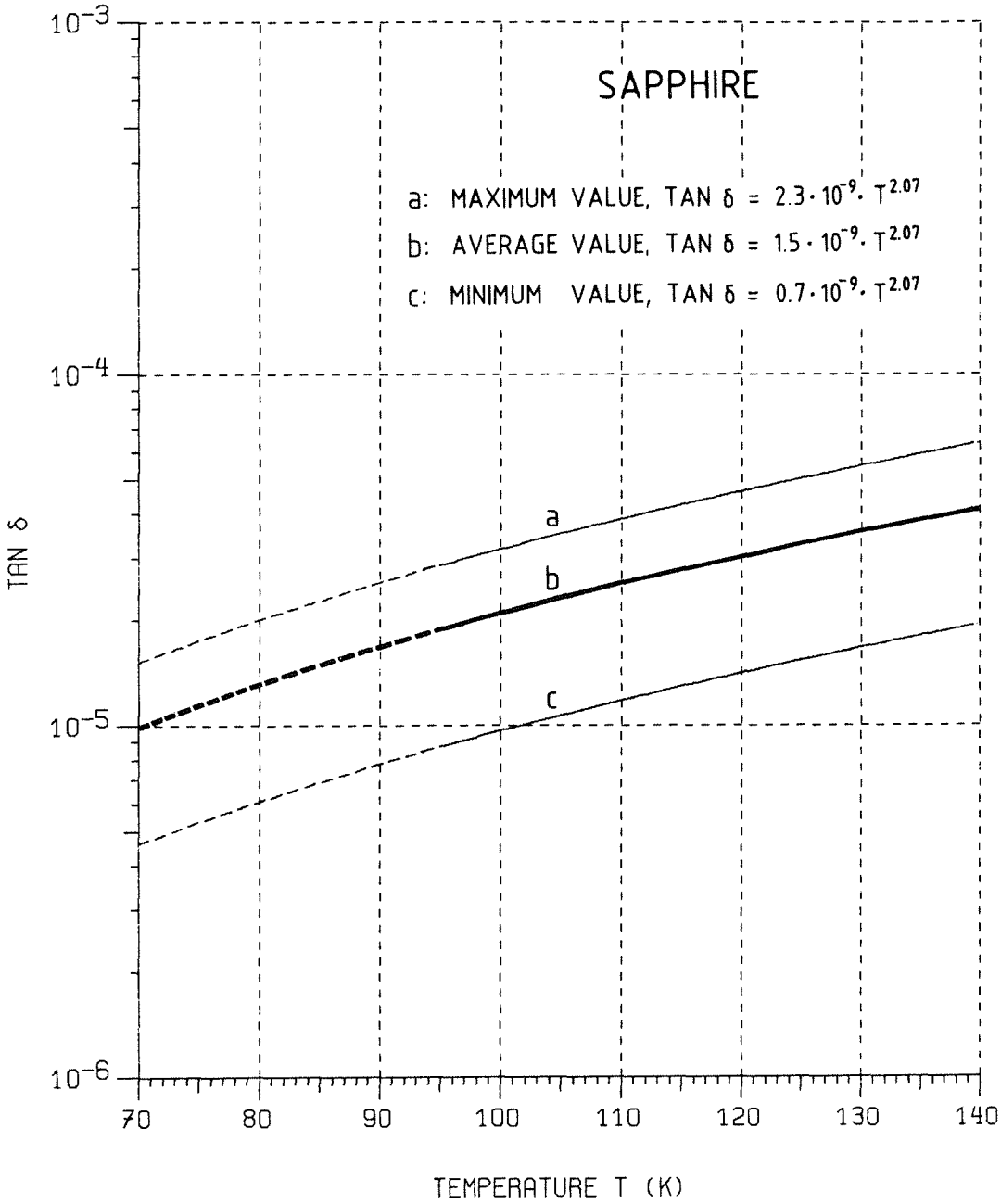

Fig. 4 Loss tangent of sapphire with an approximate measurement error range for temperatures between 70 and 140 K

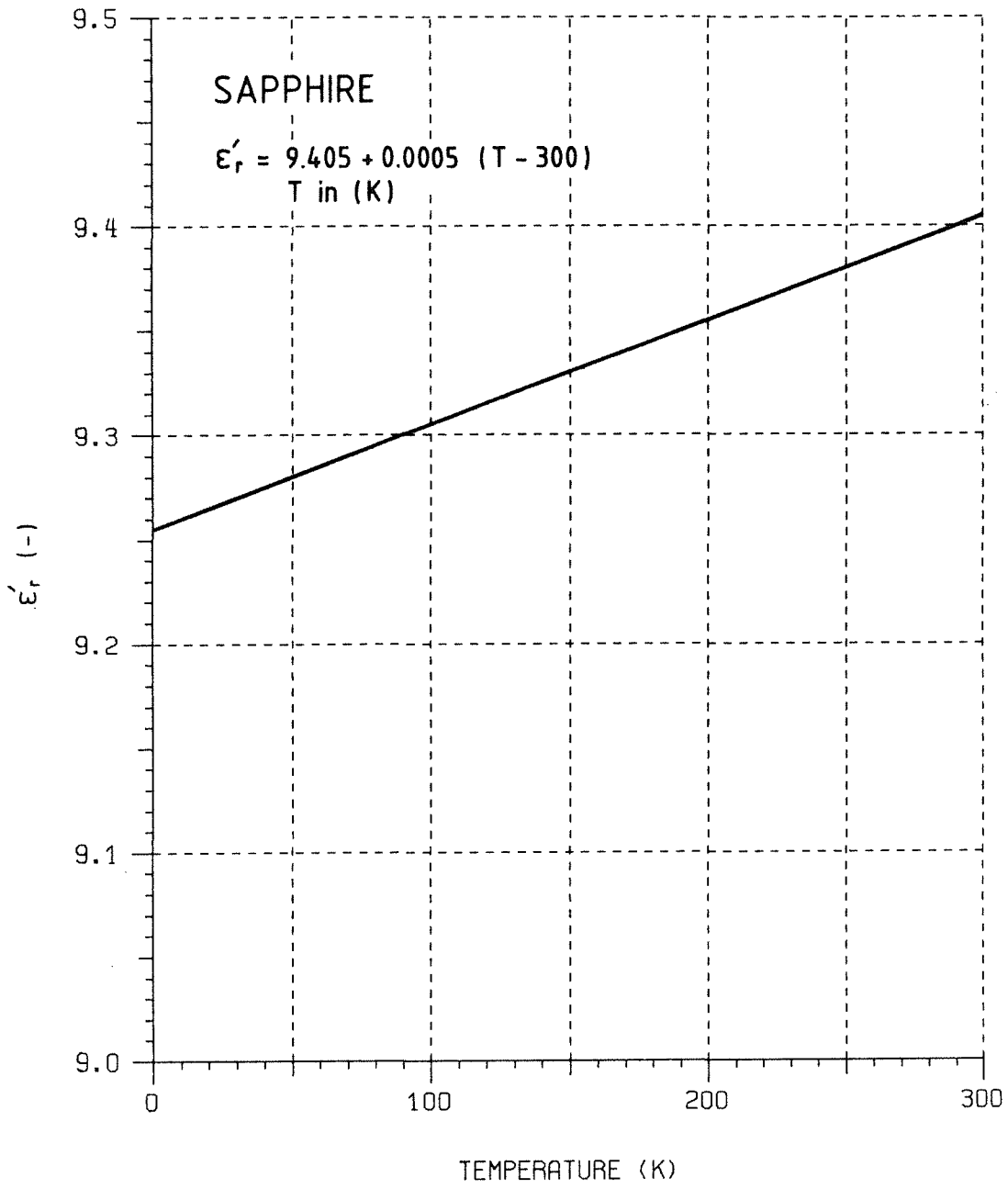

Fig. 5 Dielectric constant for sapphire /3/

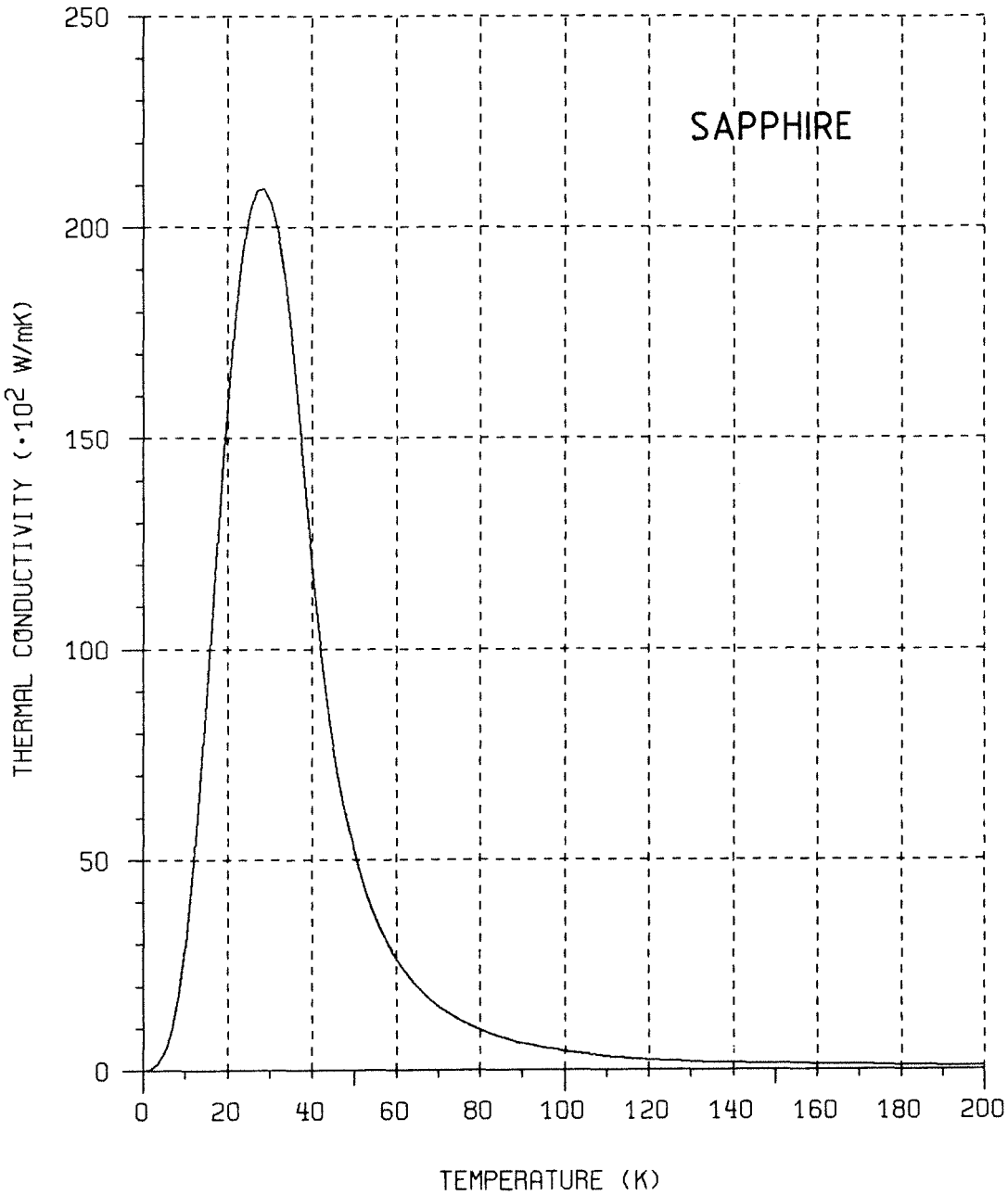

Fig. 6 Thermal conductivity of sapphire /4/

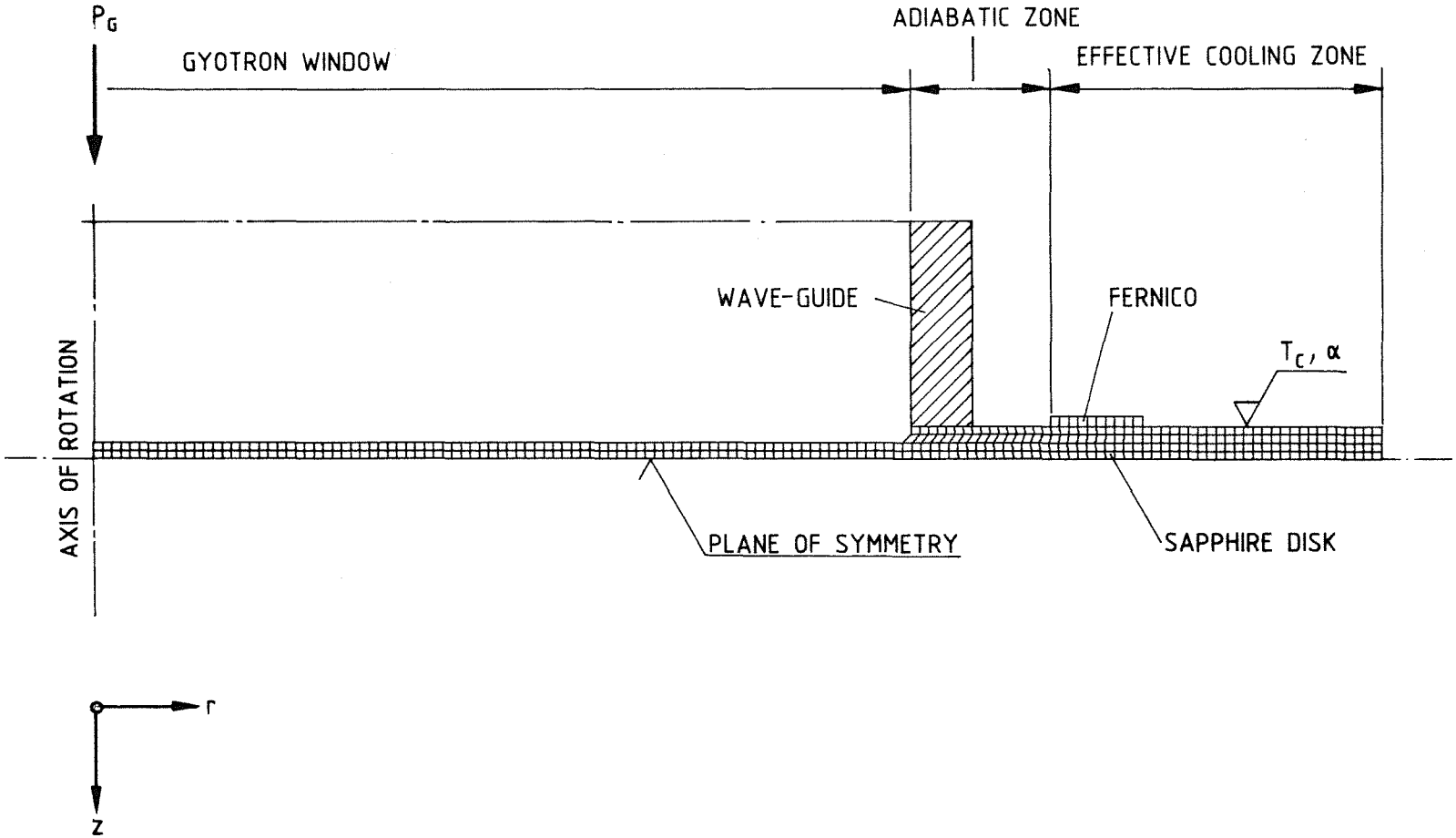

Fig. 7 Finite-element model for ABAQUS

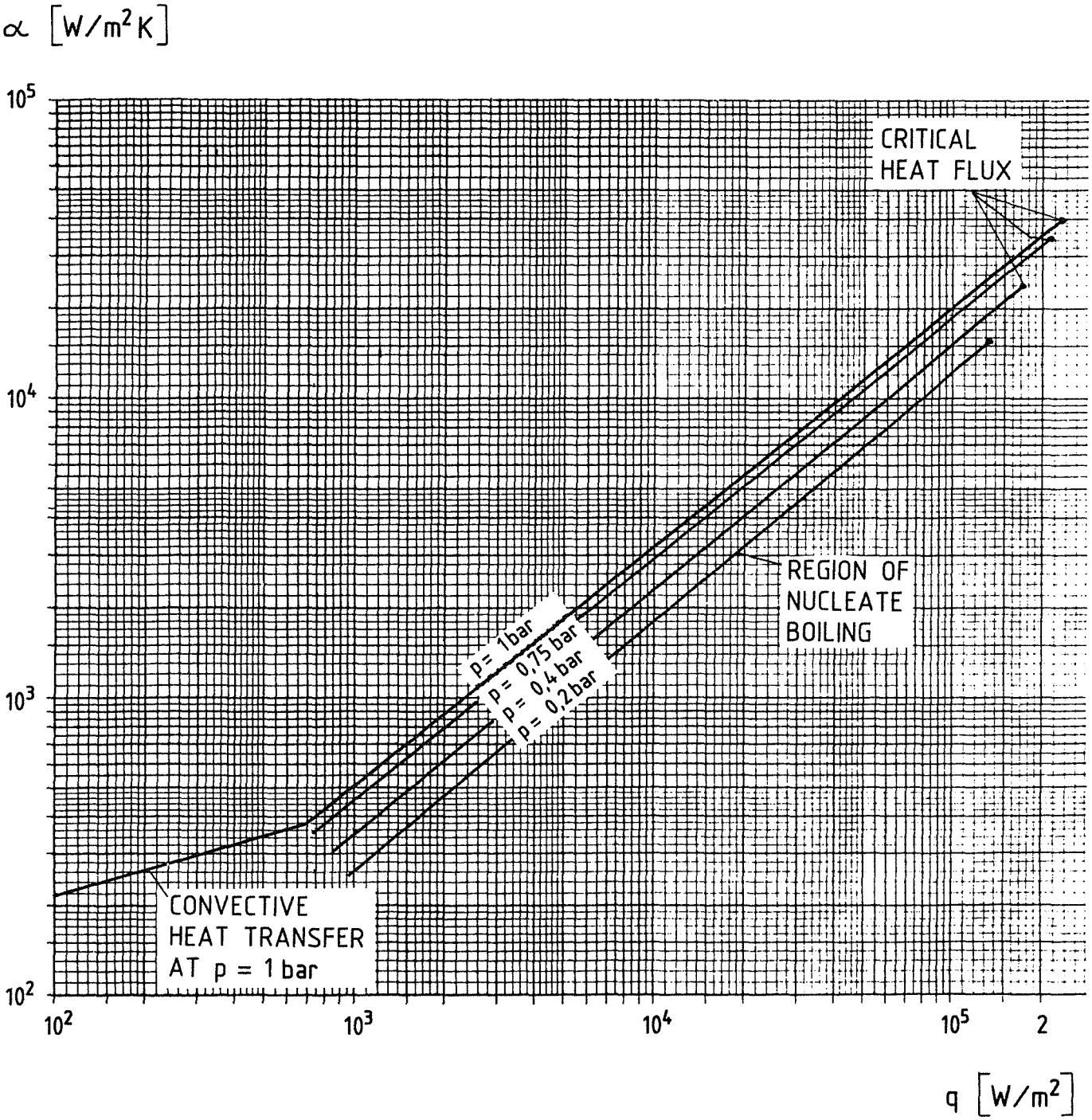

Fig. 8 Heat transfer coefficient, α, as a function of the surface heat flux density, q.

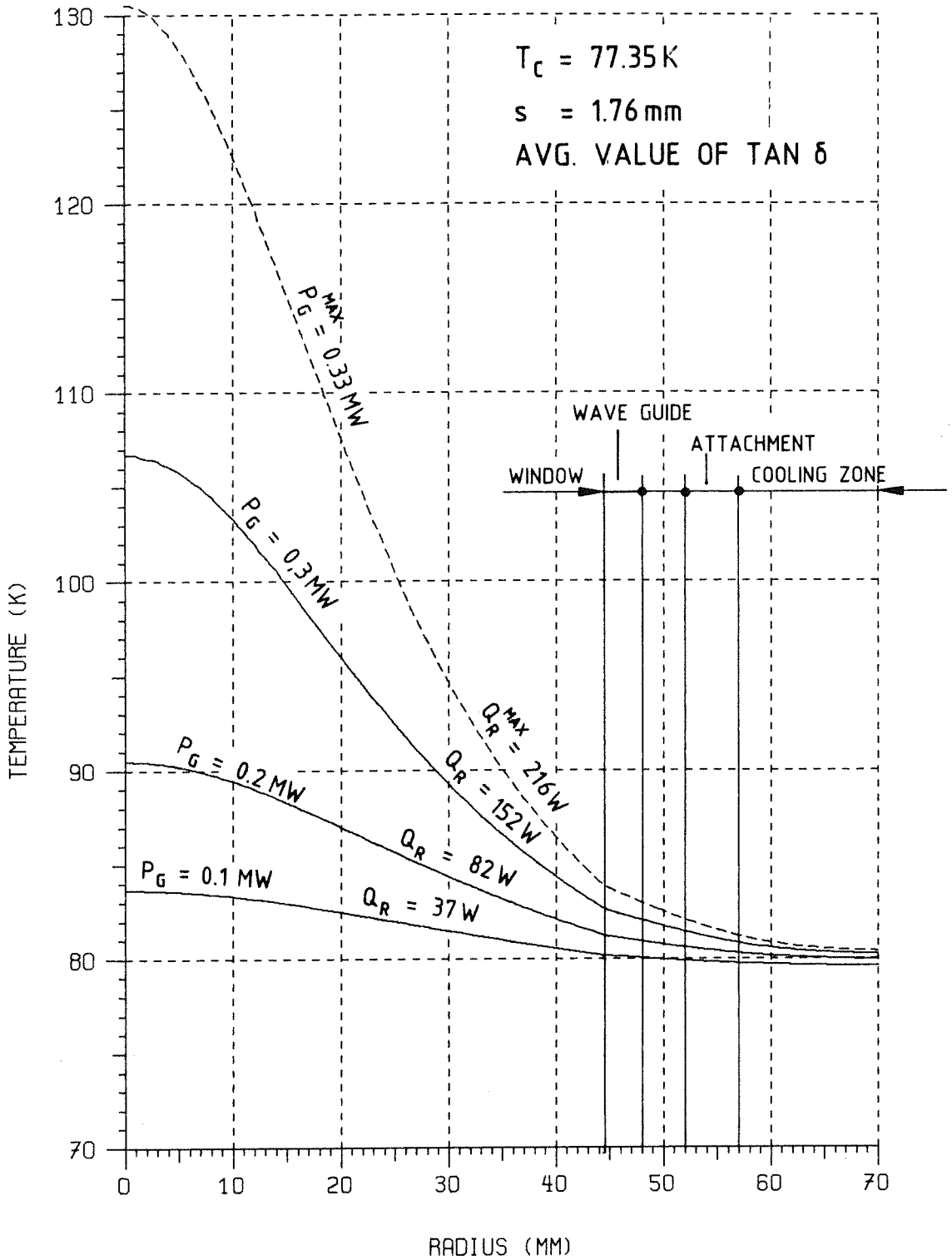

Fig. 9 Radial temperature distribution in the window in the reference case as a function of gyrotron power

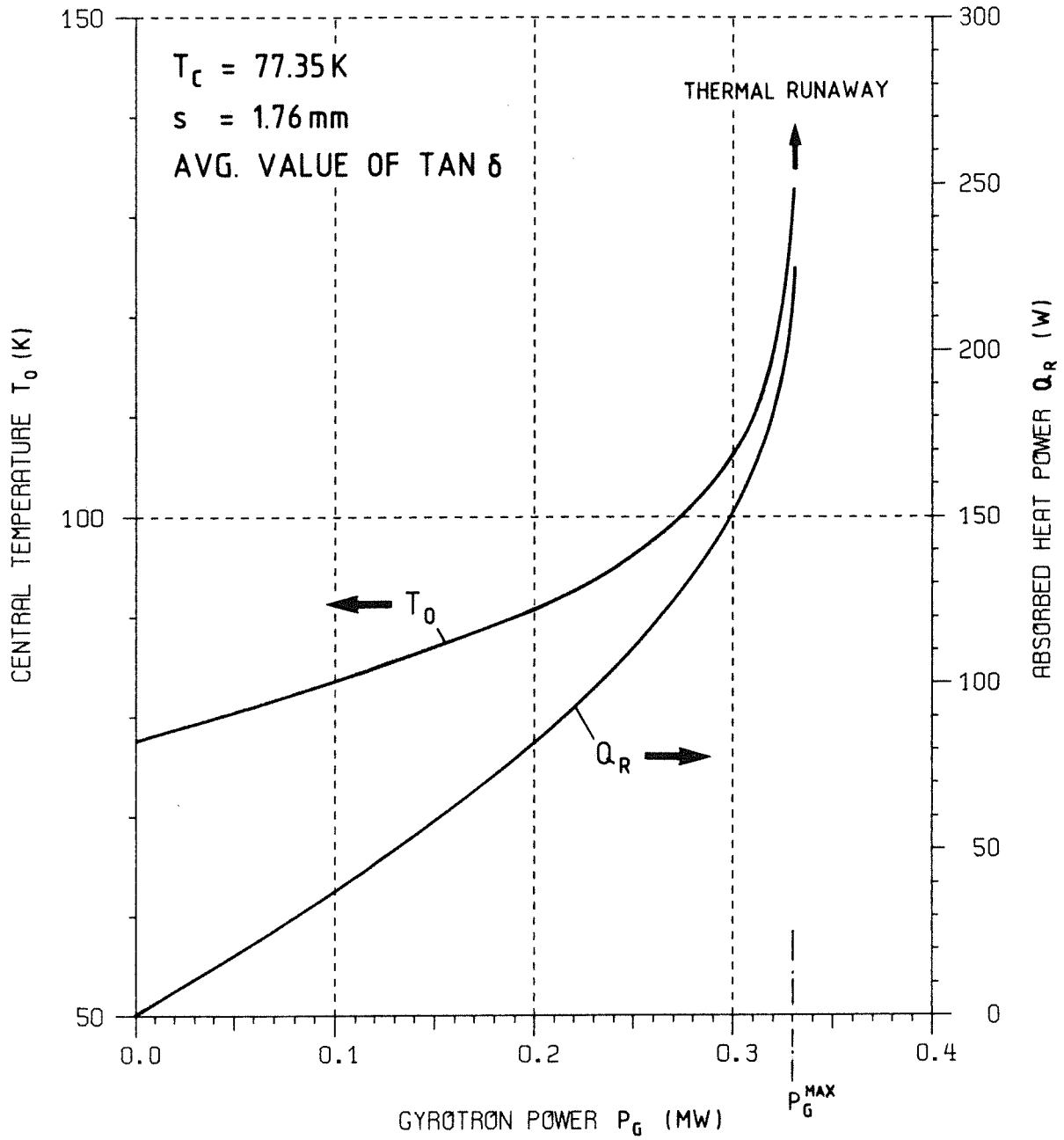

Fig. 10 Center temperature and absorbed power as a function of the power transmitted in the reference case

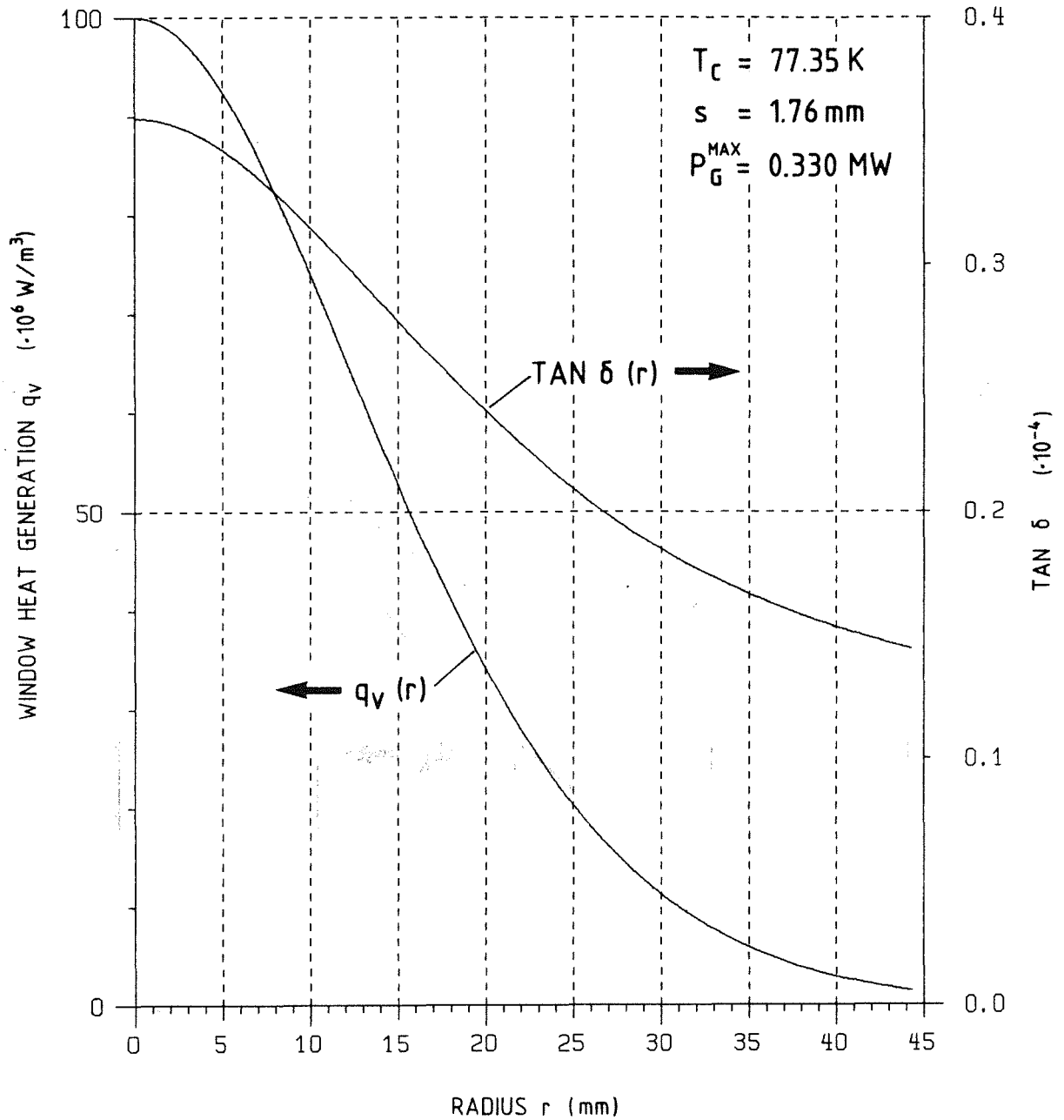

Fig. 11 Radial distribution of the loss tangent and of the thermal power density resulting at P_G^{max} in the reference case

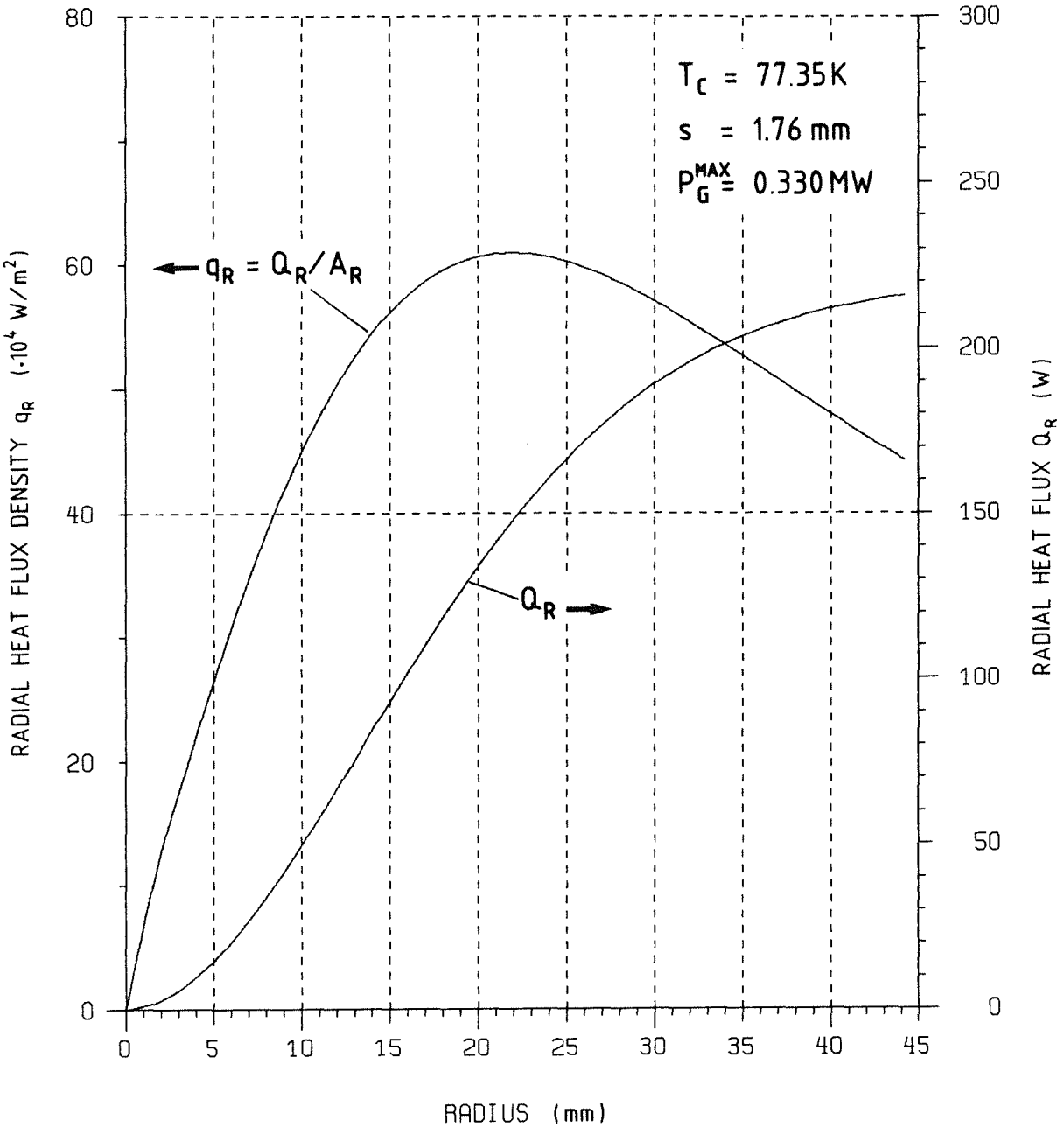

Fig. 12 Curve of the thermal power dissipated radially and the normalized heat flux density resulting at P_G^{max} in the reference case

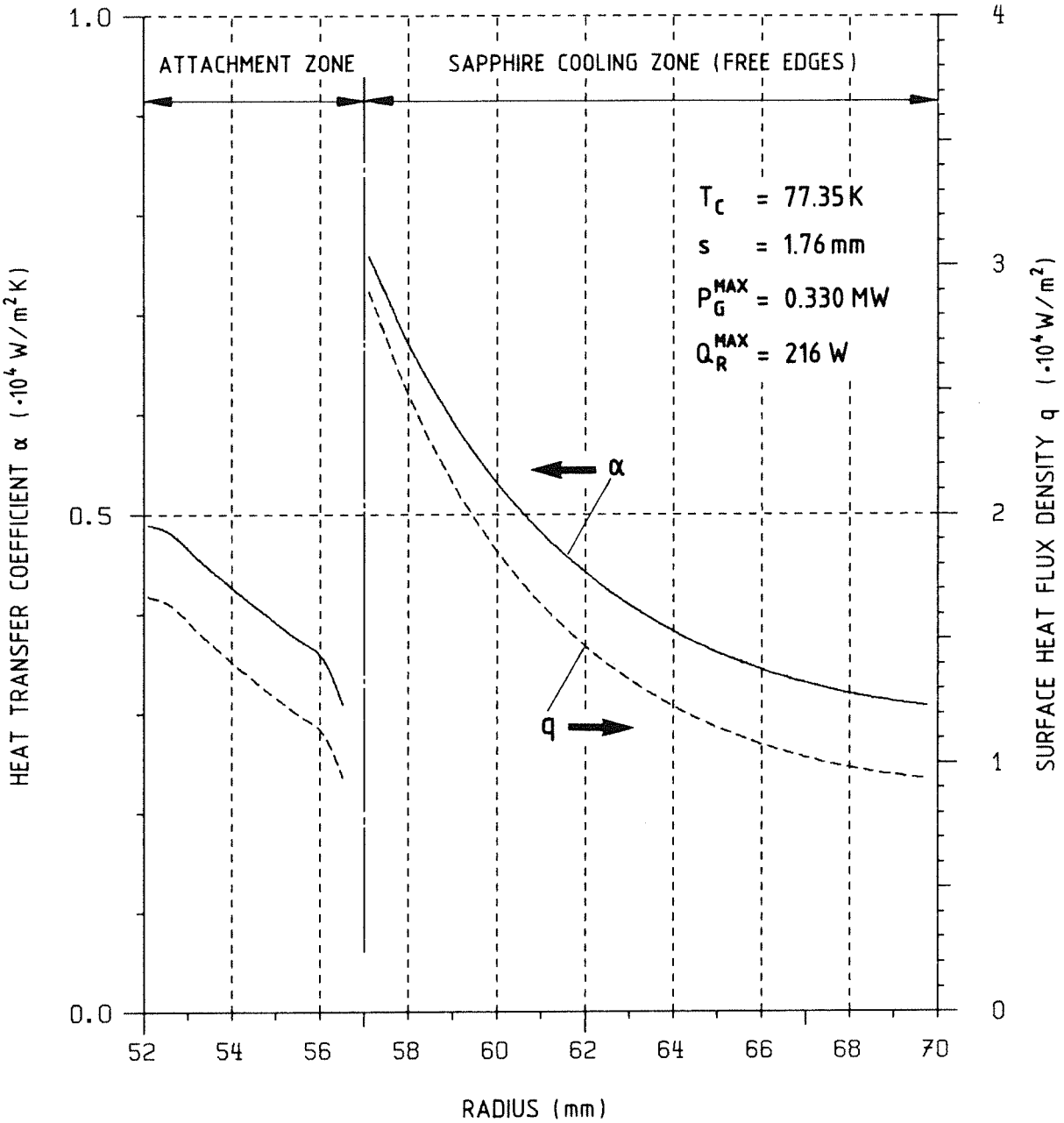

Fig. 13 Curve of the surface heat flux density and the heat transfer coefficient in the cooled zone resultant at P_G^{max} in the reference case

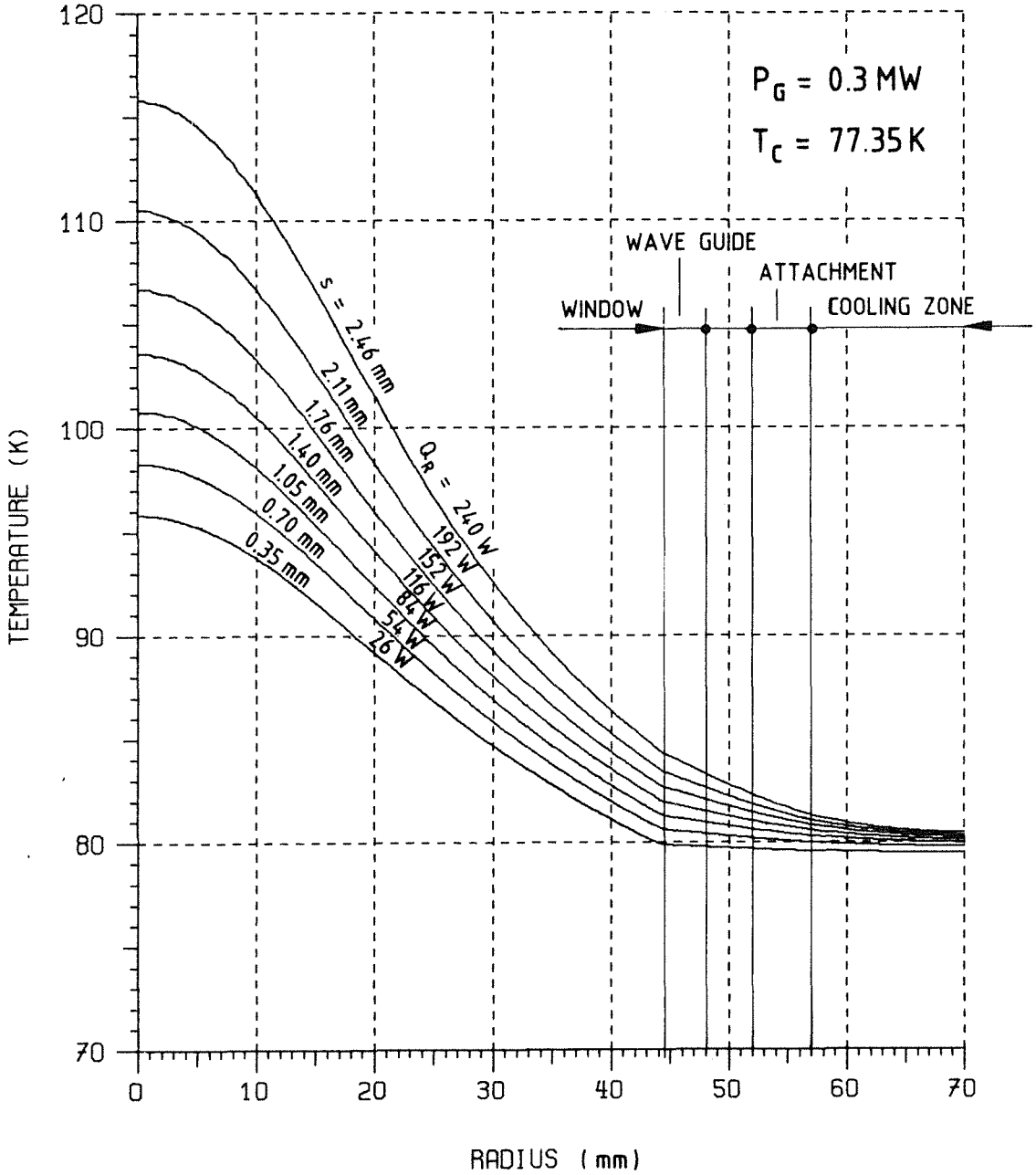

Fig. 14 Influence of the window thickness on the temperature distribution in the window

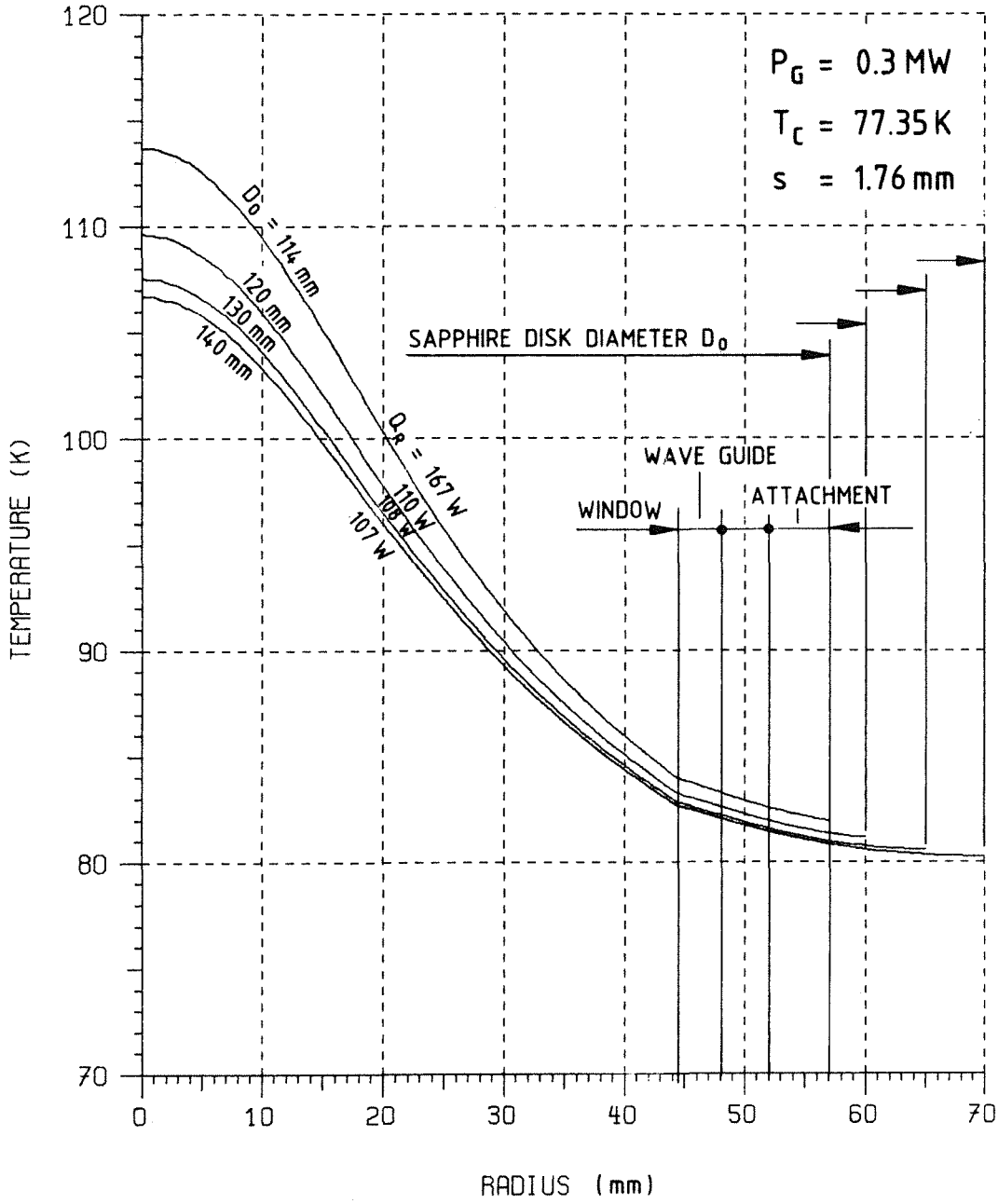

Fig. 15 Influence of the size of the sapphire upon the temperature distribution in the window

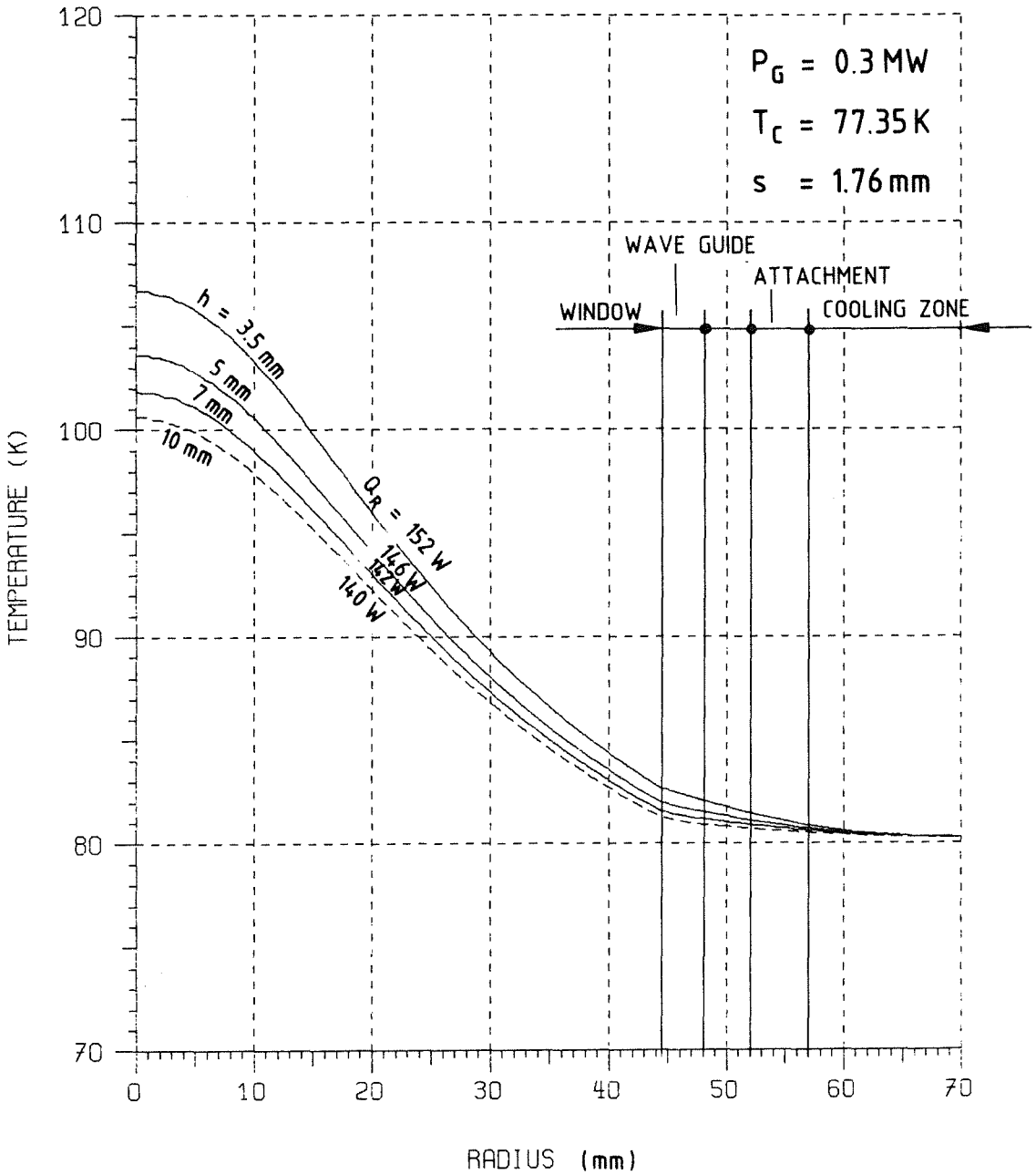

Fig. 16 Influence of the thickness of the window edge upon the temperature distribution in the window

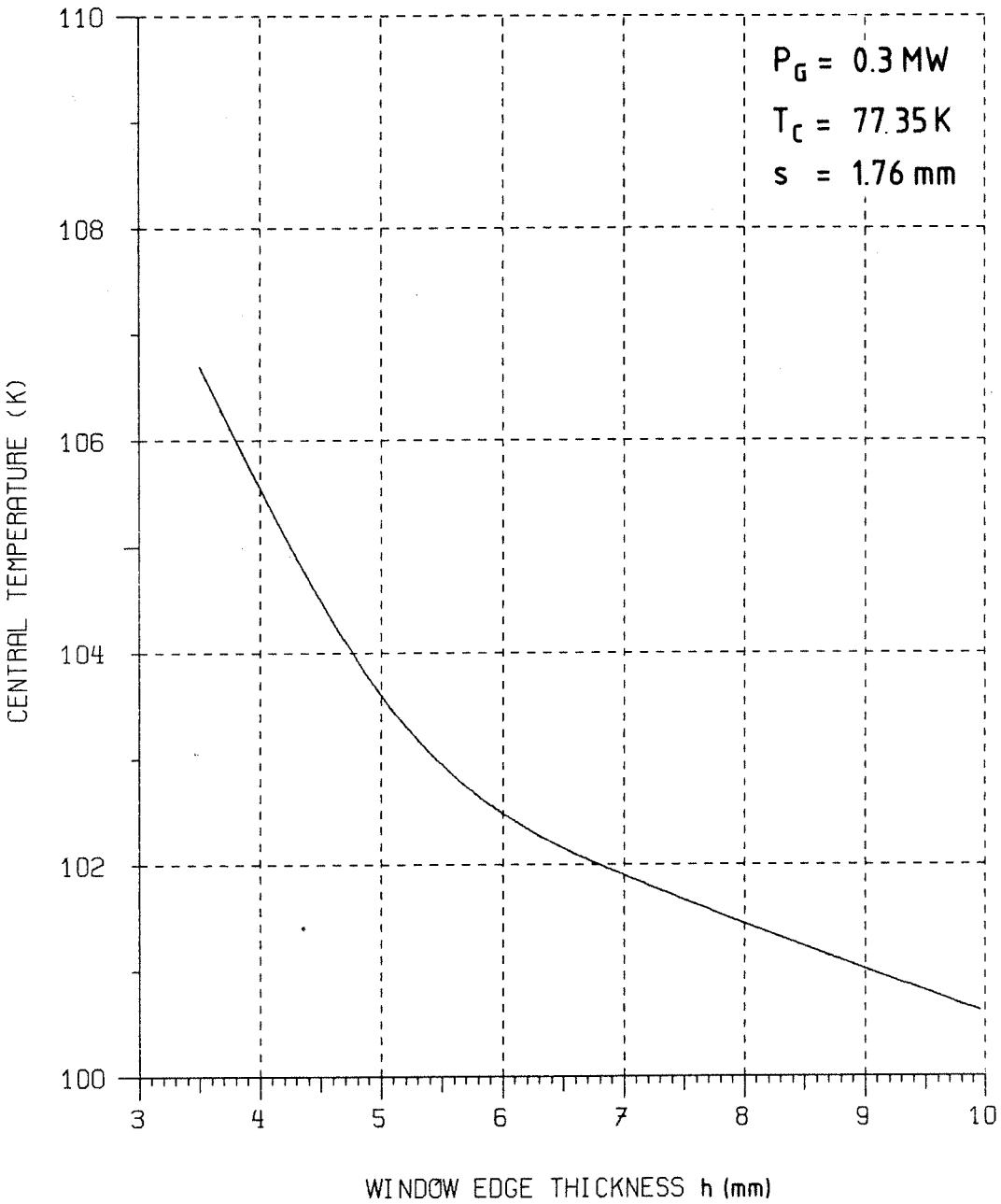

Fig. 17 Center temperature of the windos as a function of the thickness of the window edge in accordance with Fig. 16

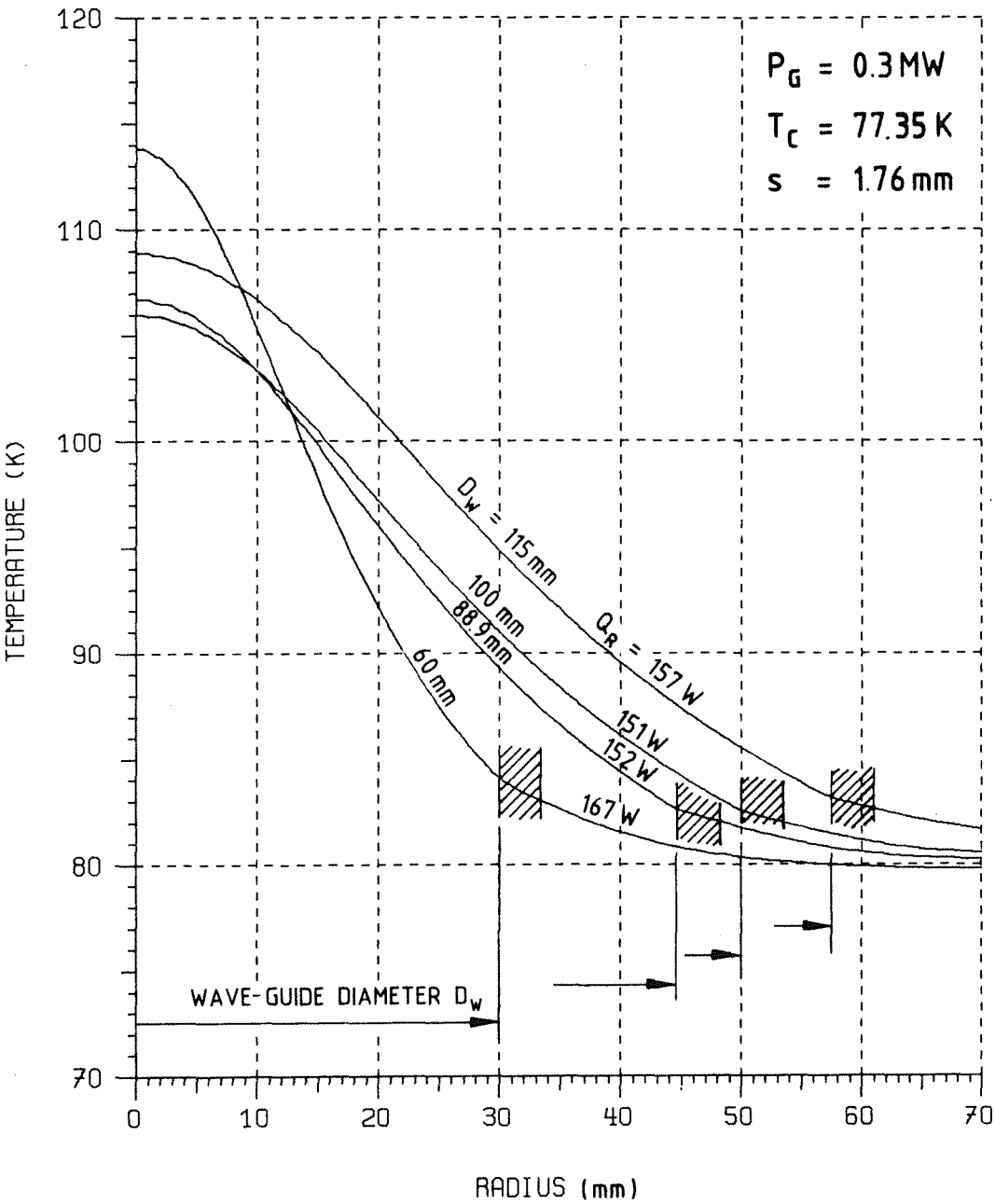

Fig. 18 Influence of the waveguide diameter upon the temperature distribution in the window

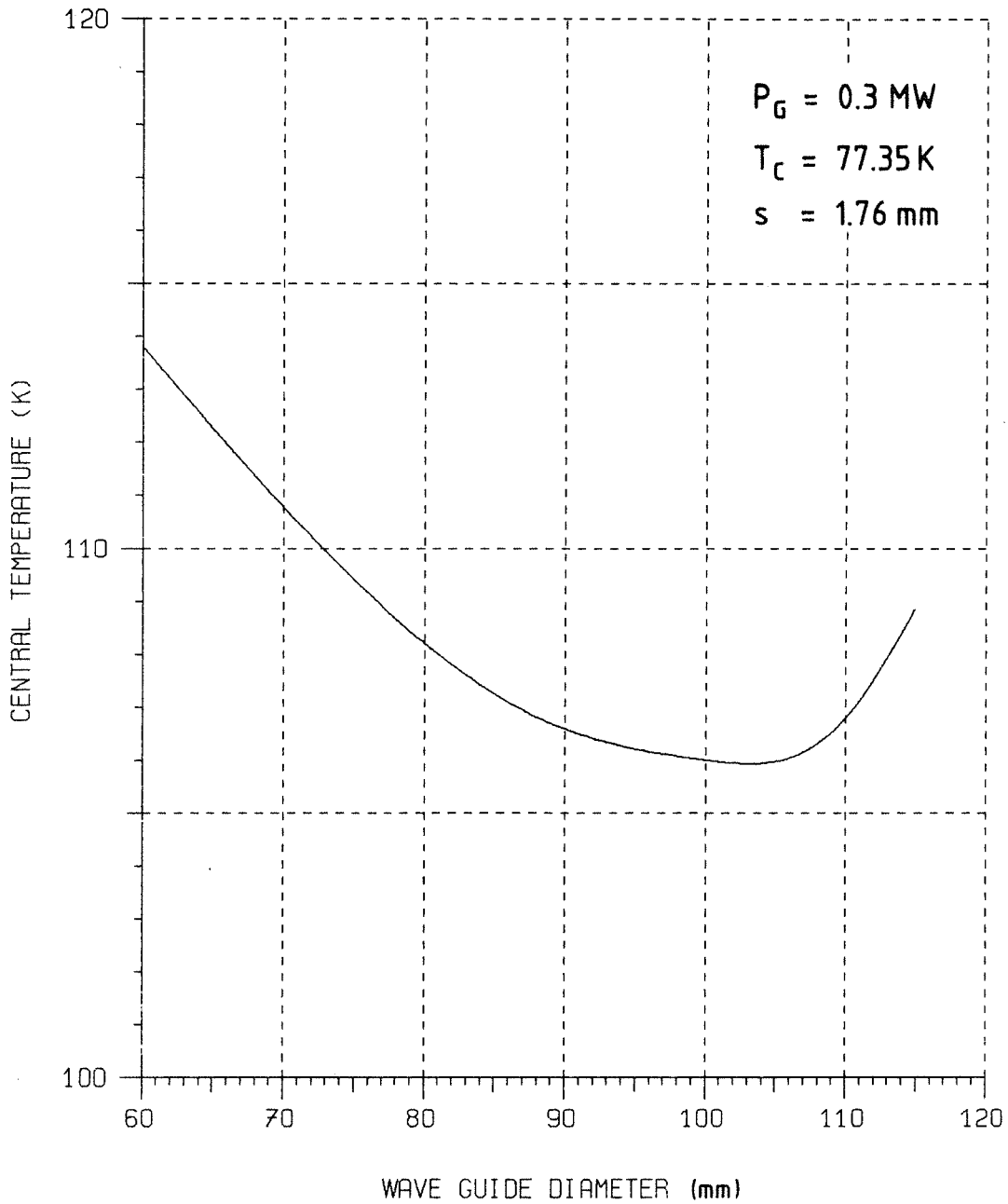

Fig. 19 Center temperature of the window as a function of the waveguide diameter in accordance with Fig. 18

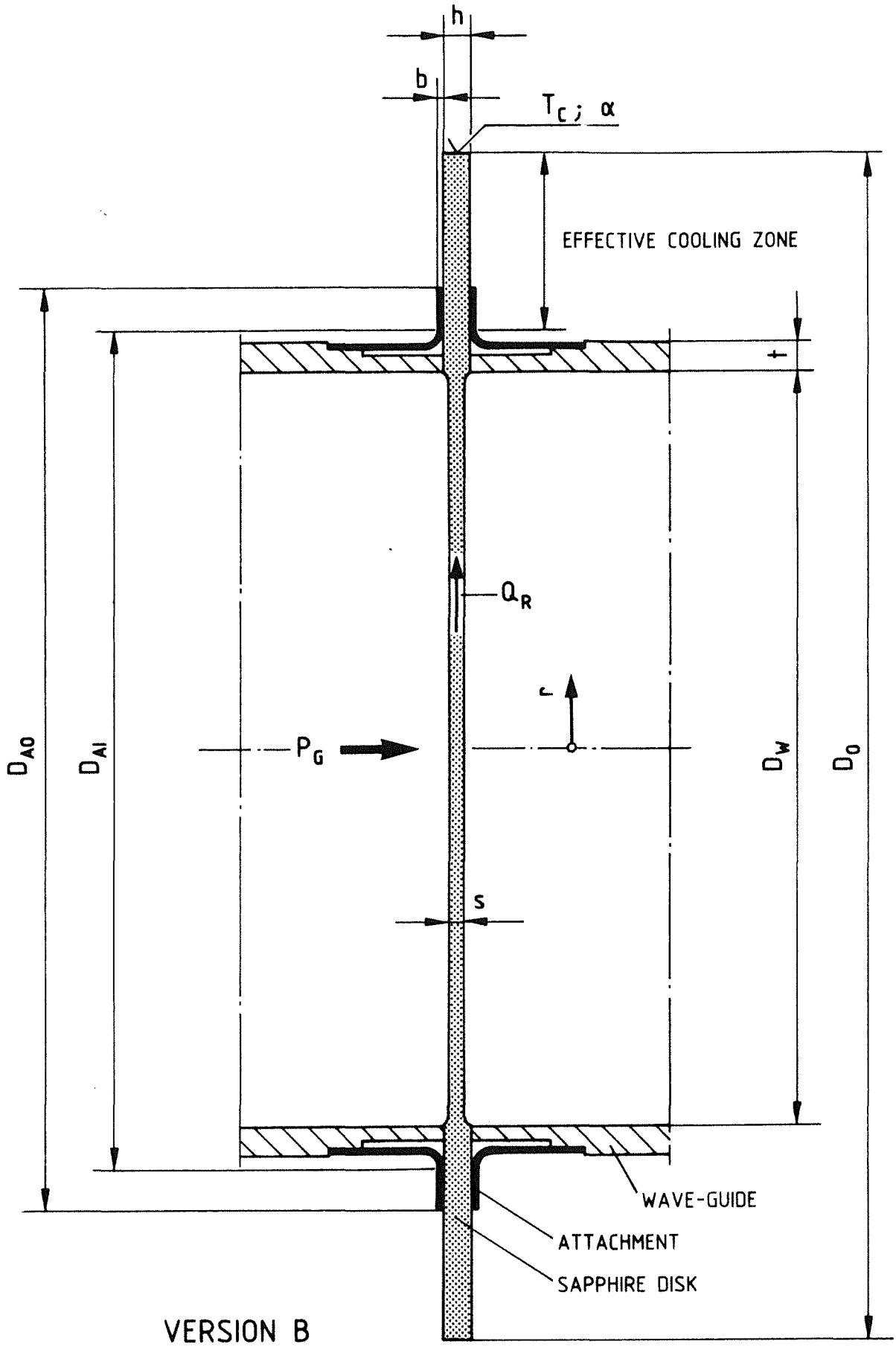

Fig. 20 Version B of the flat-collar window geometry

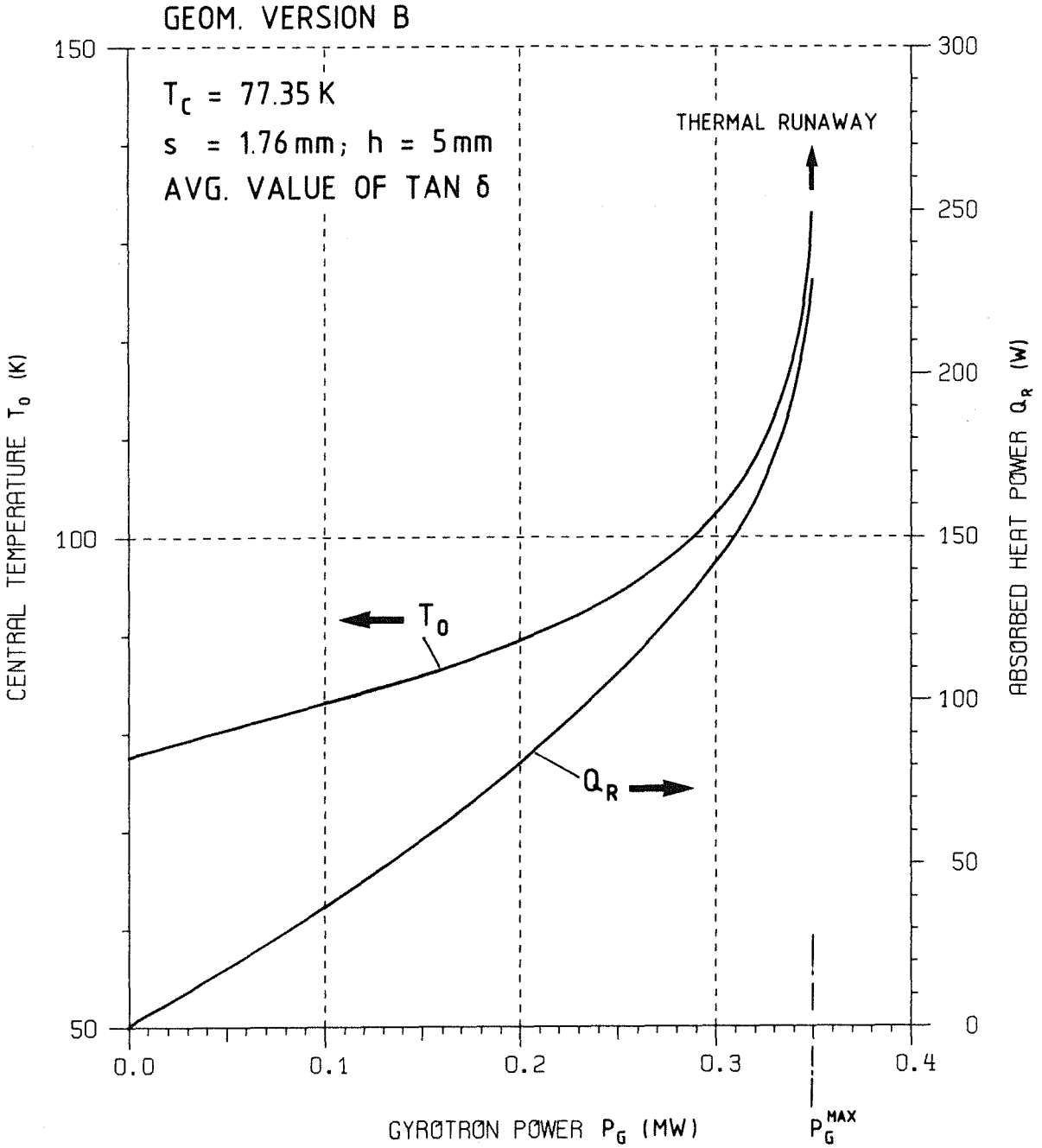

Fig. 21 Center temperature and absorbed power as a function of the power transmitted in the version B collar geometry with h=5 mm and under other reference conditions

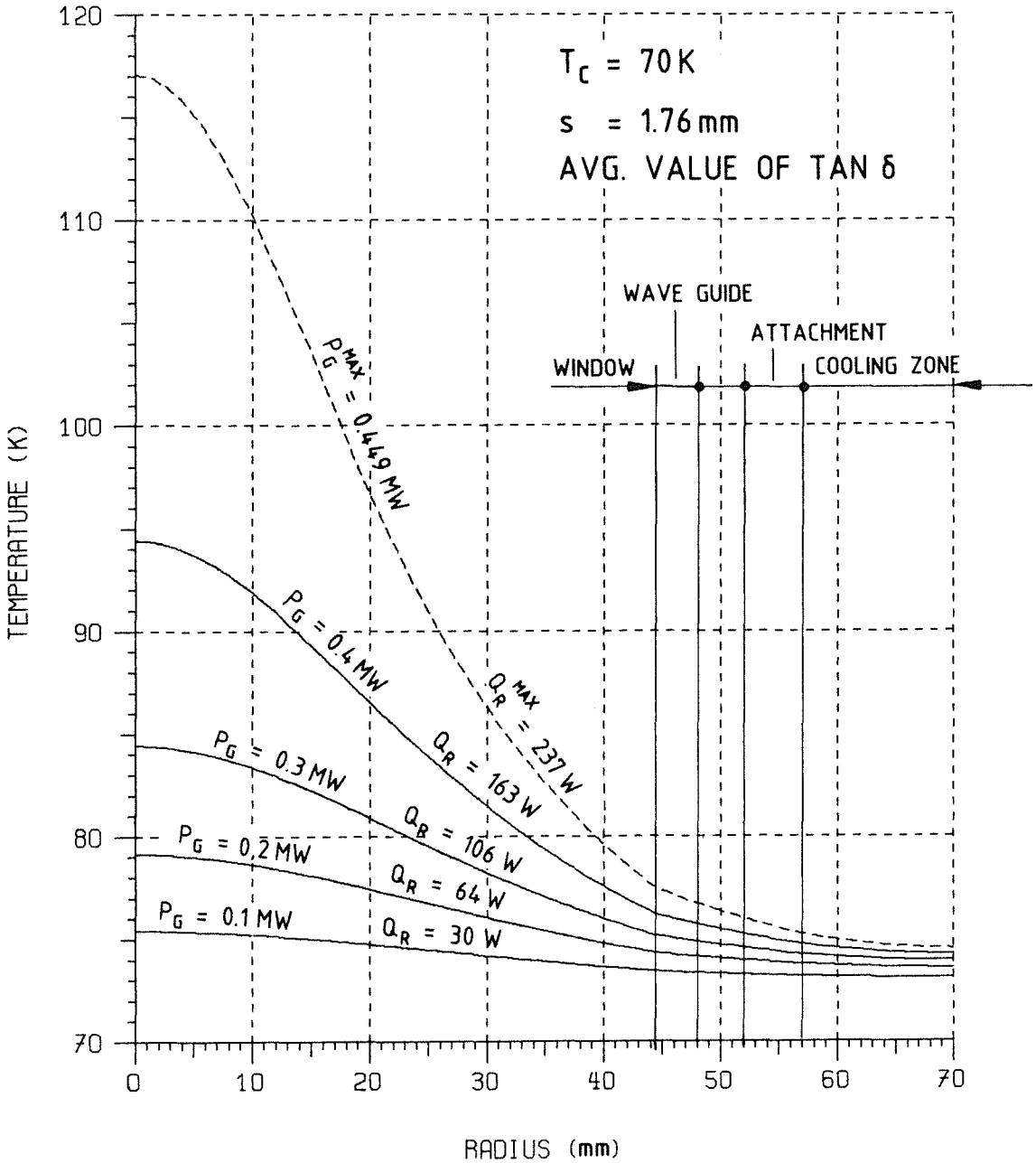

Fig. 22 Radial temperature distribution in the window of reference geometry at a coolant temperature of 70 K and medium tan δ values

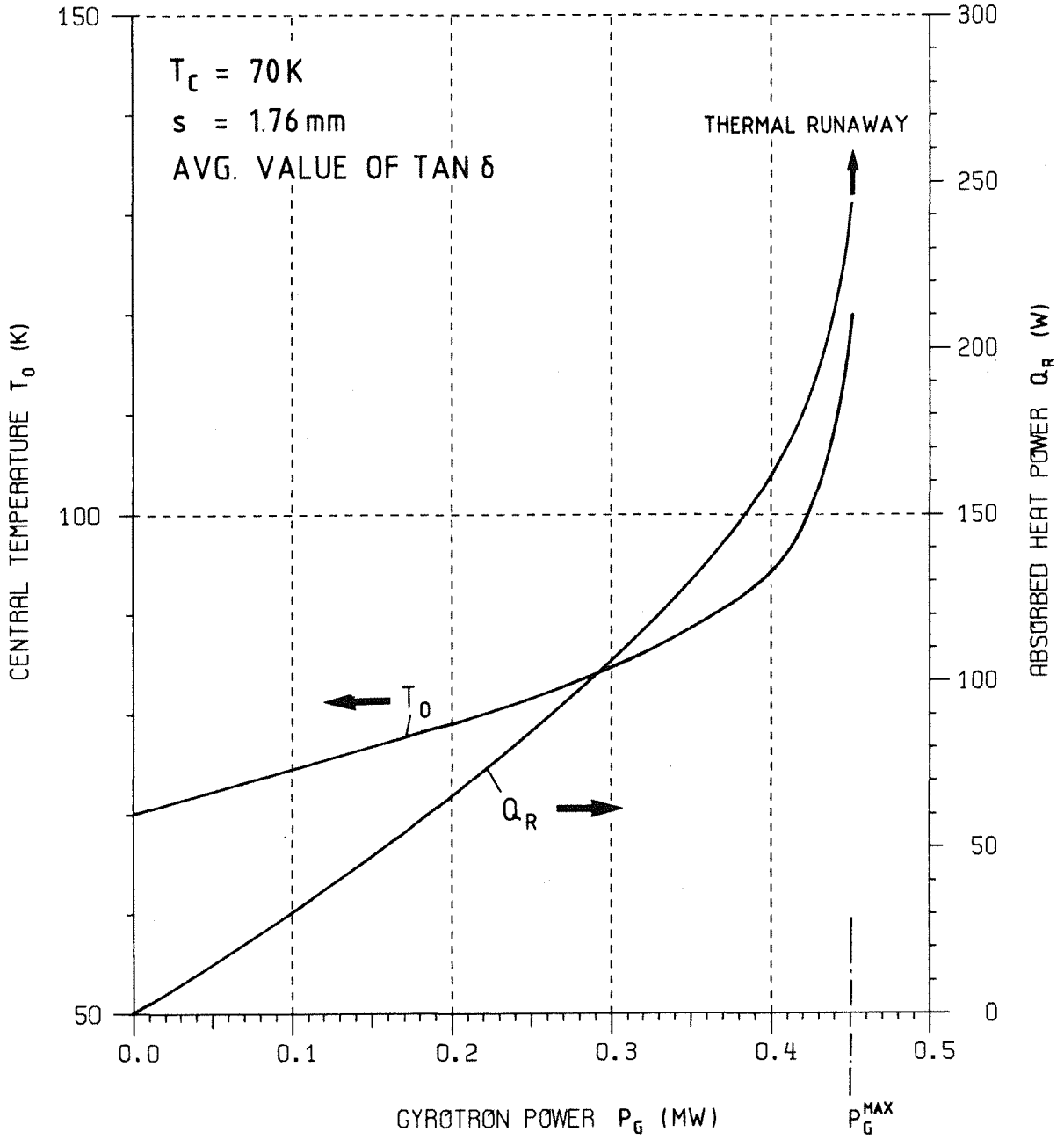

Fig. 23 Center temperature and absorved power as a function of gyrotron power for the reference geometry with T_C = 70 K and medium tan δ values

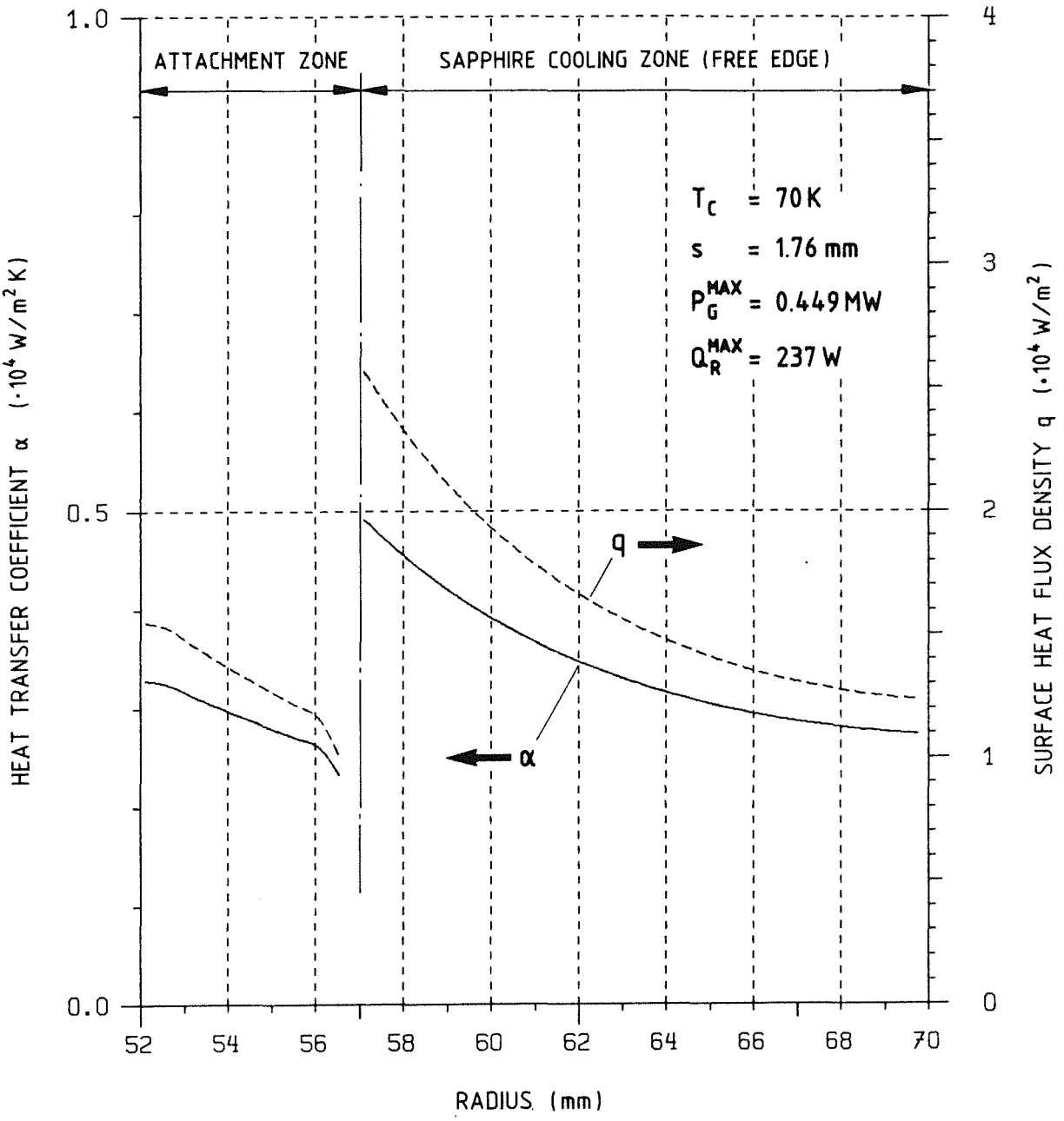

Fig. 24 Curves of q and α in the cooled zone at P_G^{max} in accordance with Fig. 23

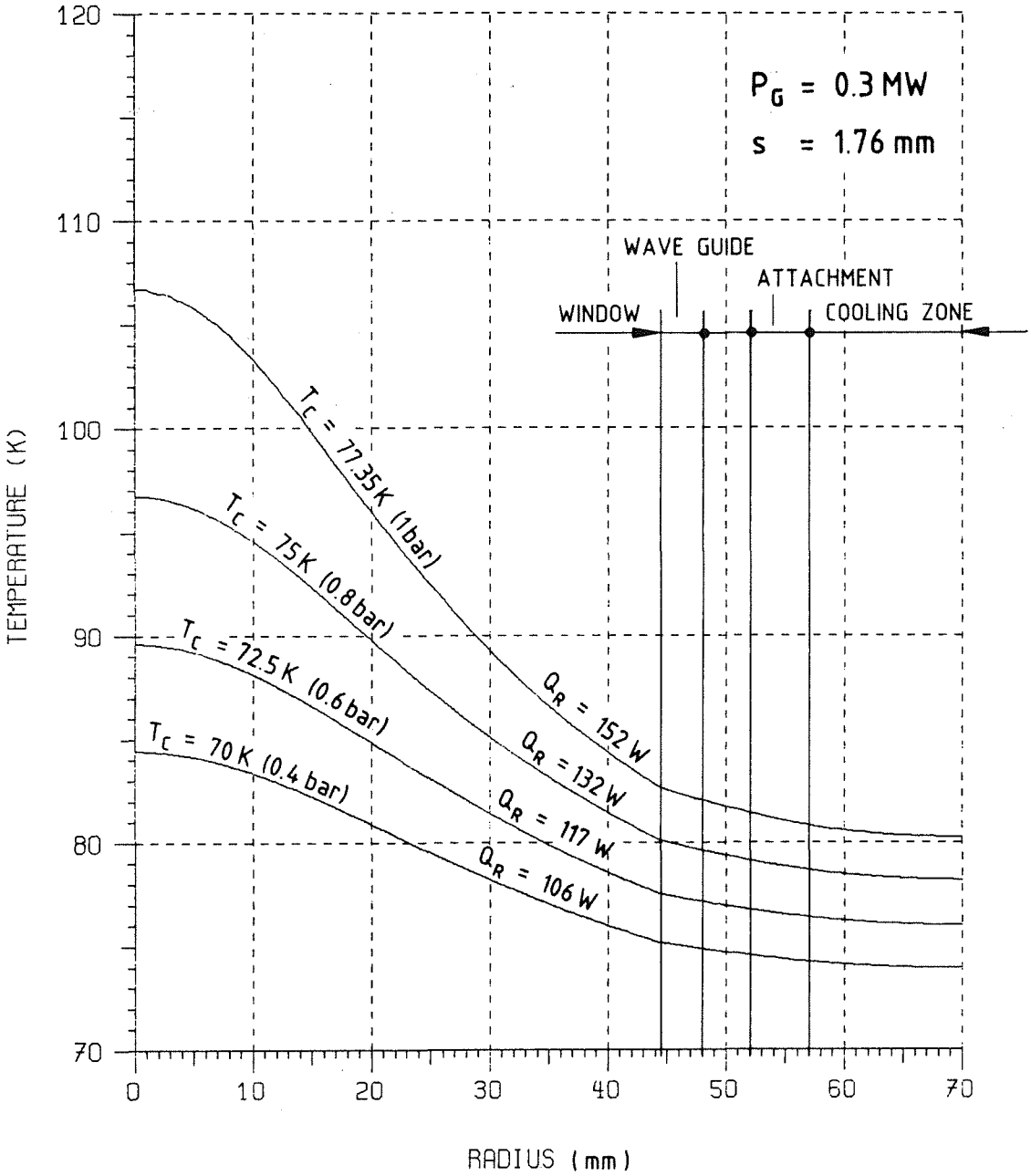

Fig. 25 Influence of the coolant temperature upon the temperature distribution in the window of reference geometry at P_G = 0.3 MW

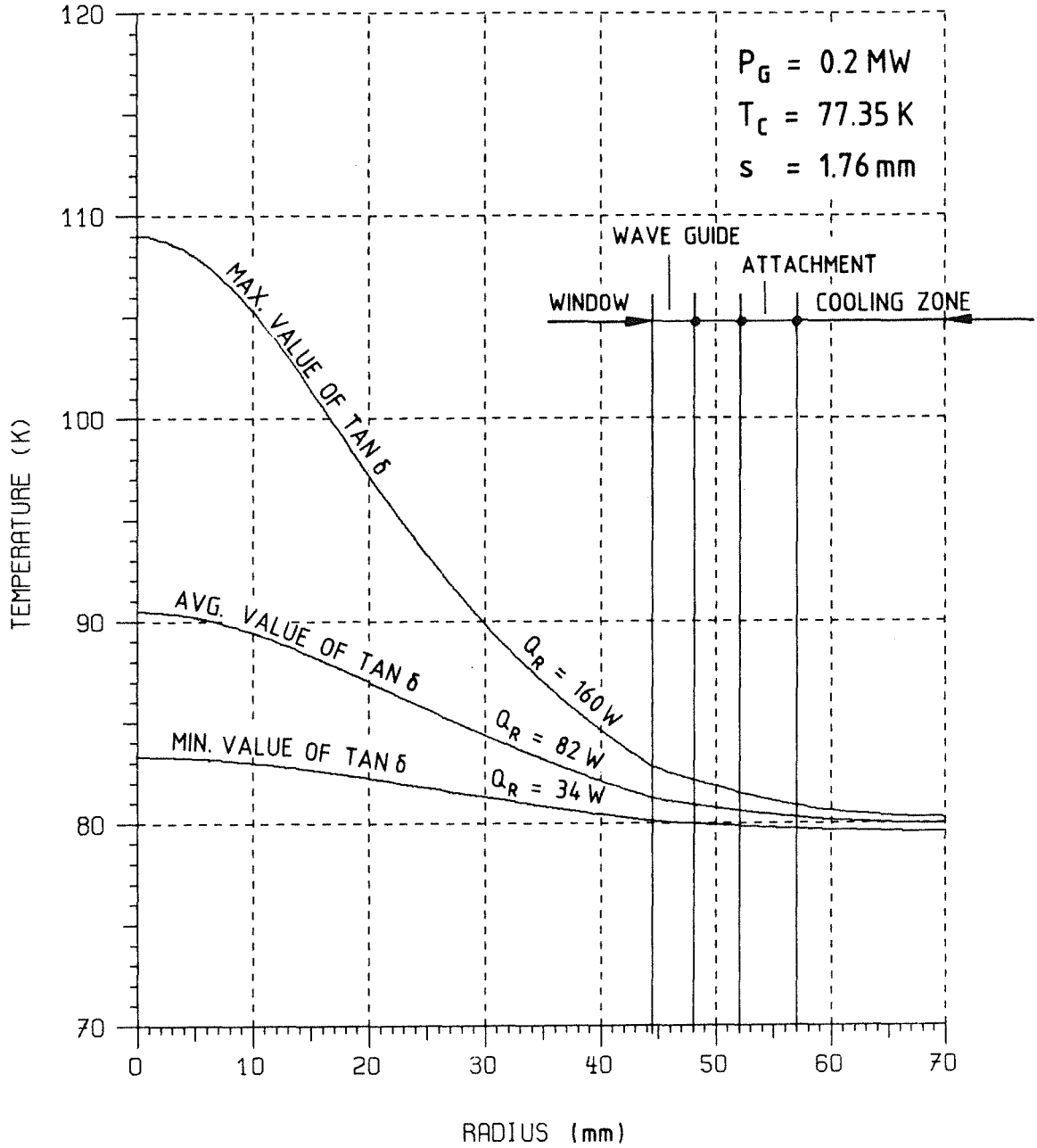

Fig. 26 Radial temperature distribution in the window for various values of tan δ on the basis of reference data and P_G = 0.2 MW

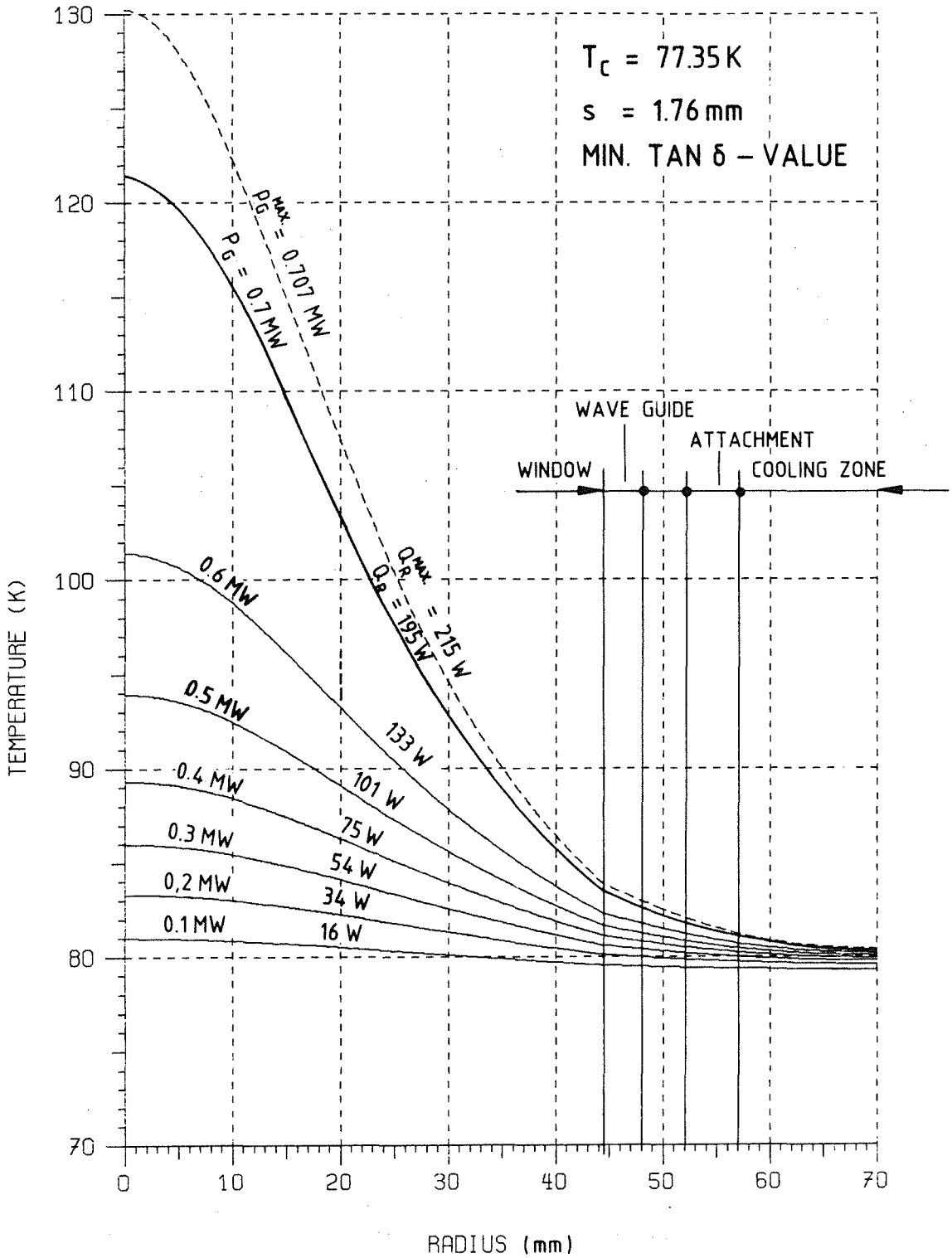

Fig. 27 Radial temperature distribution in the window of the reference data and under the assumption of minimum tan δ values

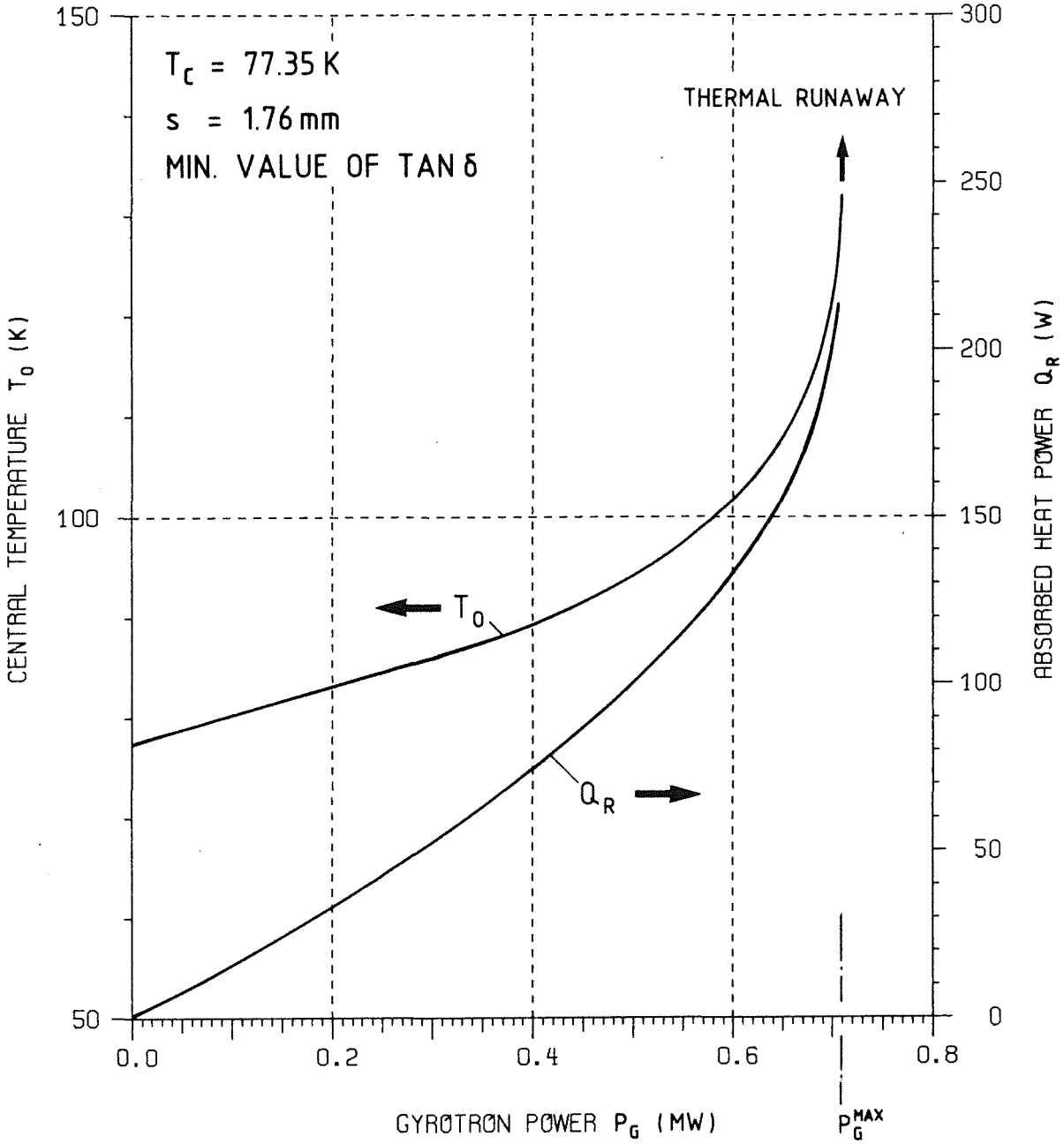

Fig. 28 Center temperature and power absorbed in the window as a function of the power transmitted for the reference geometry with minimum tan δ values and T_C = 77.35 K

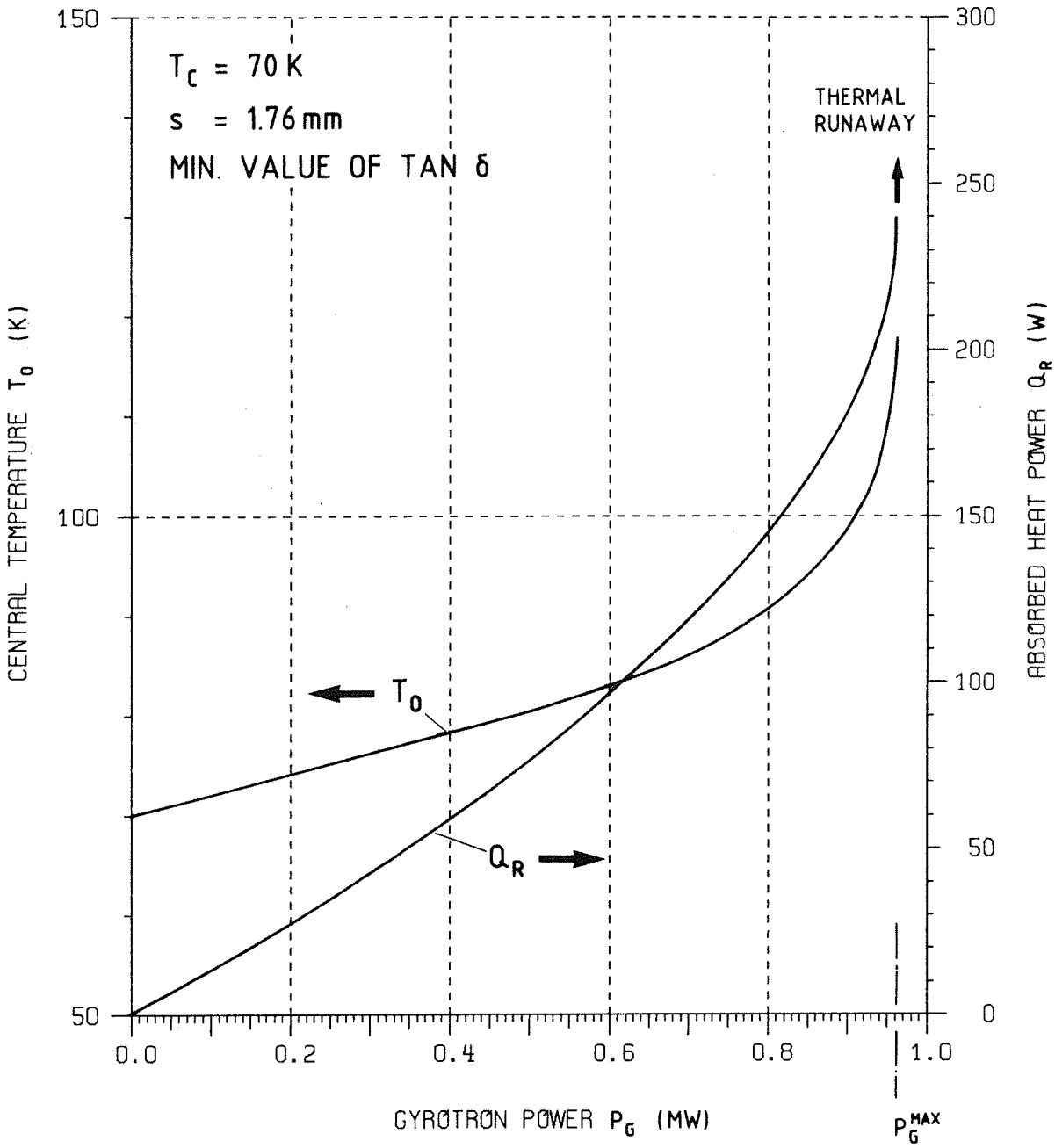

Fig. 29 Center temperature and power absorbed in the window as a function of the power transmitted for the reference geometry with minimum tan δ values and T_C = 70 K

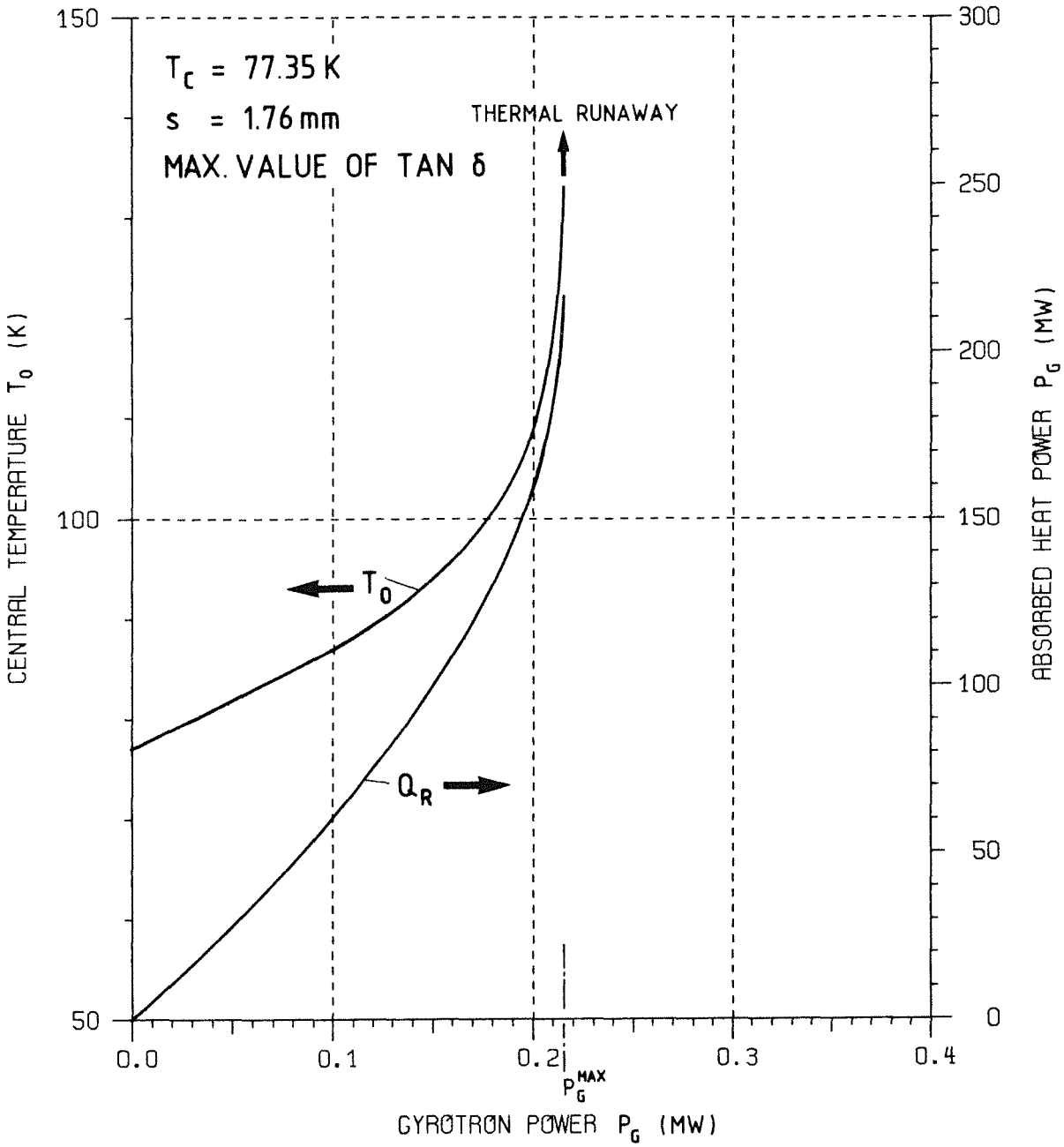

Fig. 30 Center temperature and power absorbed in the window as a function of the power transmitted for the reference geometry with maximum tan δ values and T_C = 77.35 K

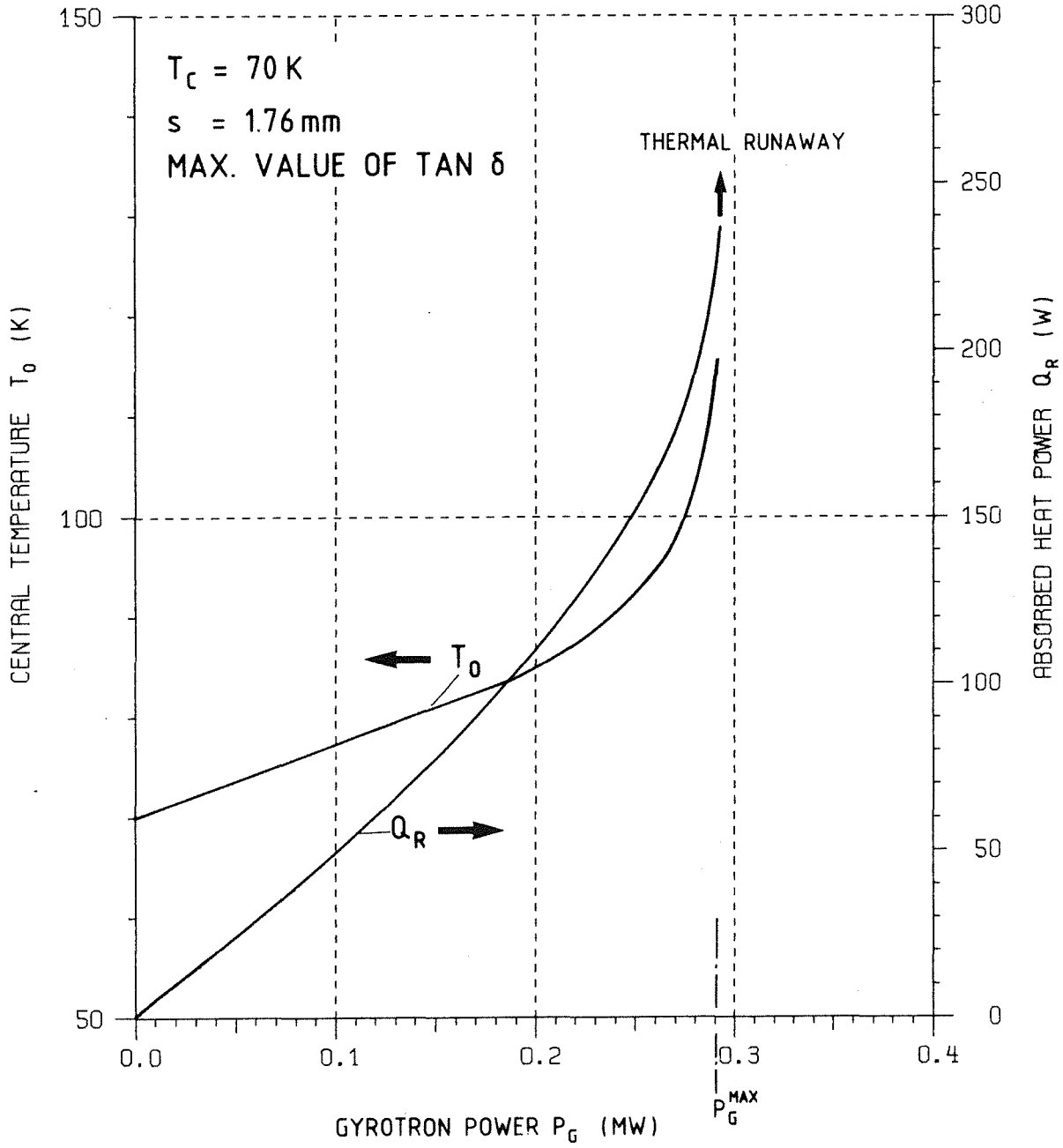

Fig. 31 Center temperature and power absorbed in the window as a function of the power transmitted for the reference geometry with maximum tan δ values and T_C = 70 K

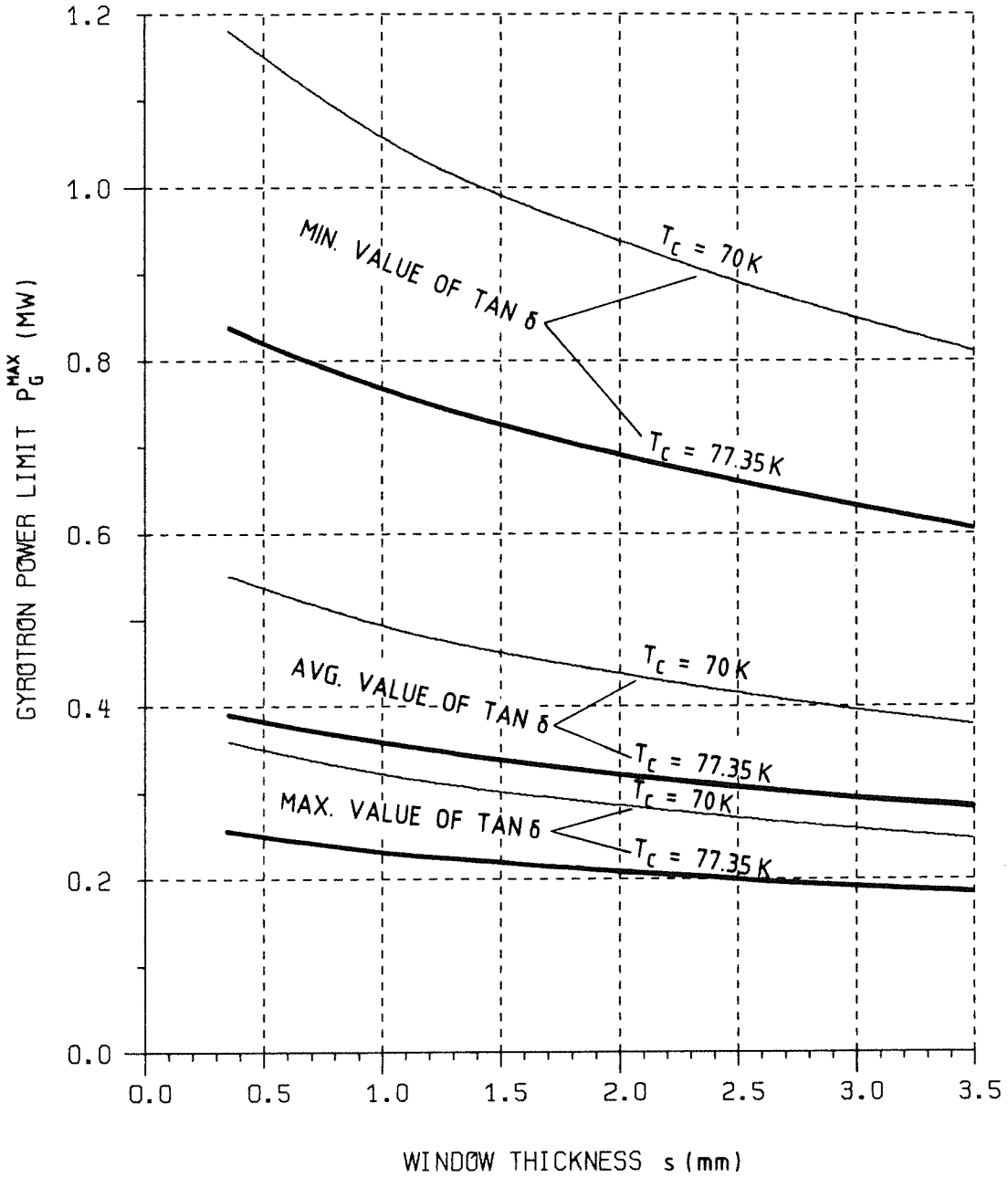

Fig. 32 Maximum power transmitted for the reference geometry as a function of the thickness of the window, the coolant temperature, and the loss tangent

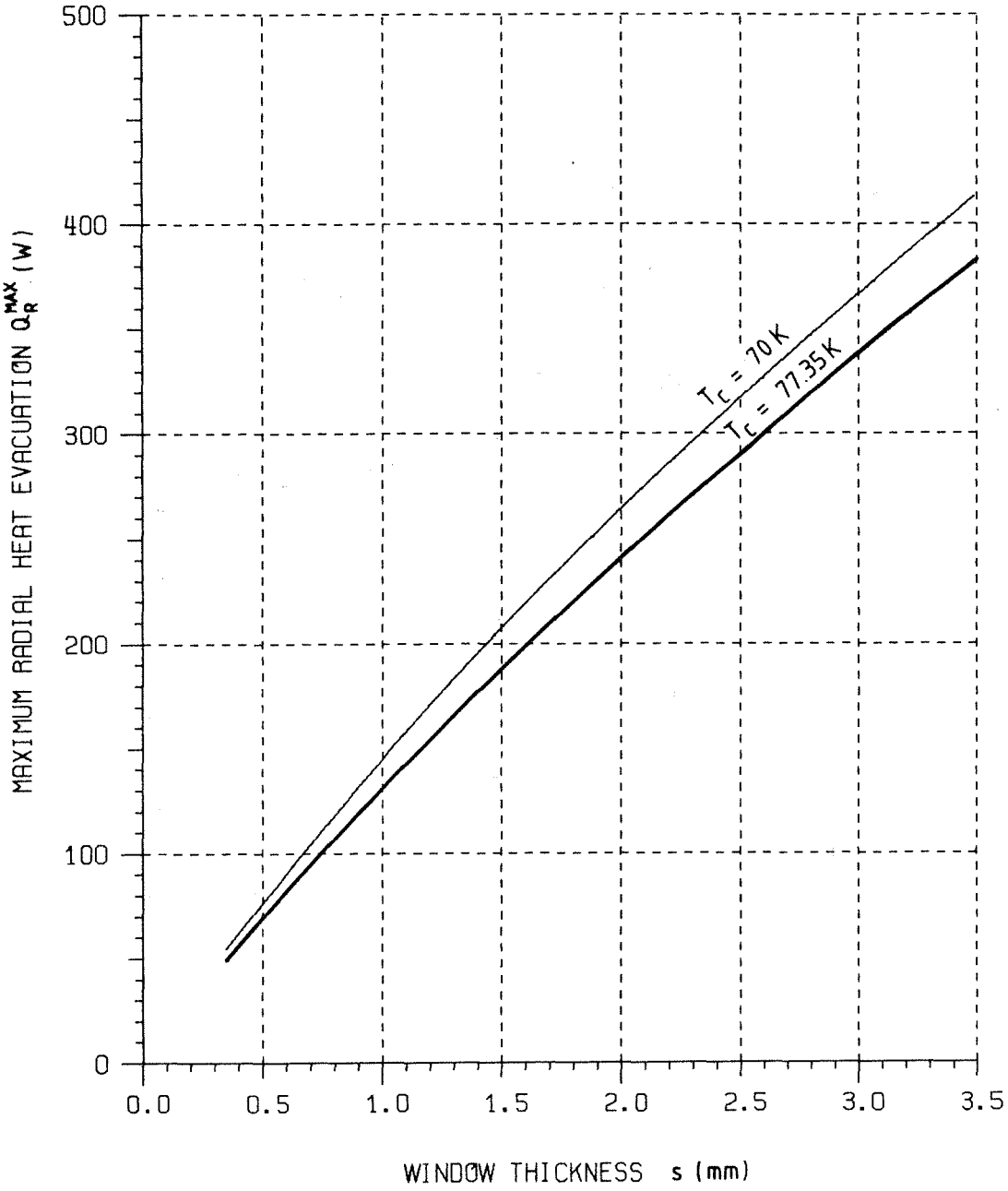

Fig. 33 Maximum radial thermal power at runaway as a function of the thickness of the window, and the coolant temperature

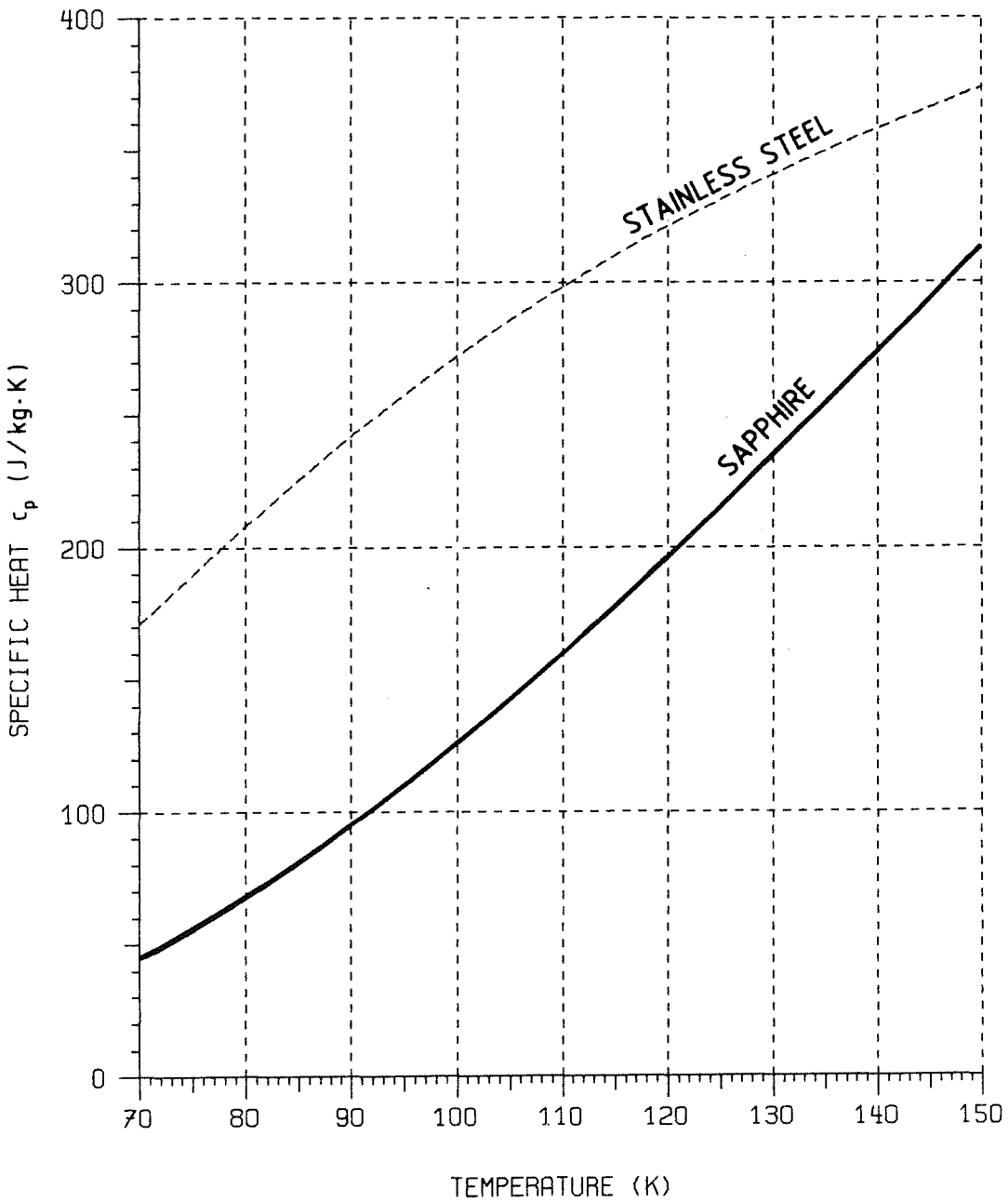

Fig. 34 Specific heat capacity of sapphire /4/ and 18/12 stainless steel /5/

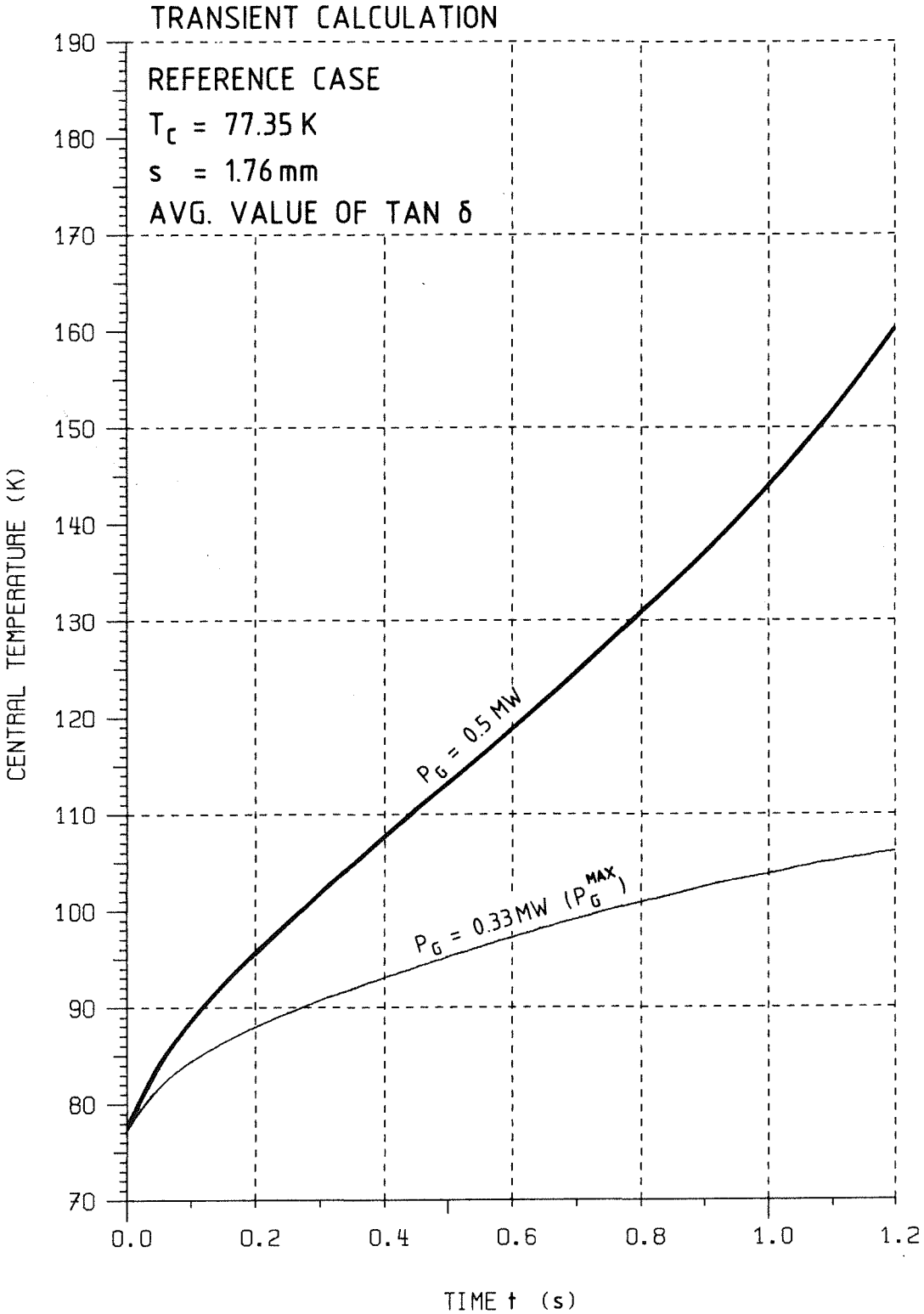

Fig. 35 Development, as a function of time, of the window center temperature in the reference case at P_G = 0.33 MW (≙ P_G^{max}) and 0.5 MW

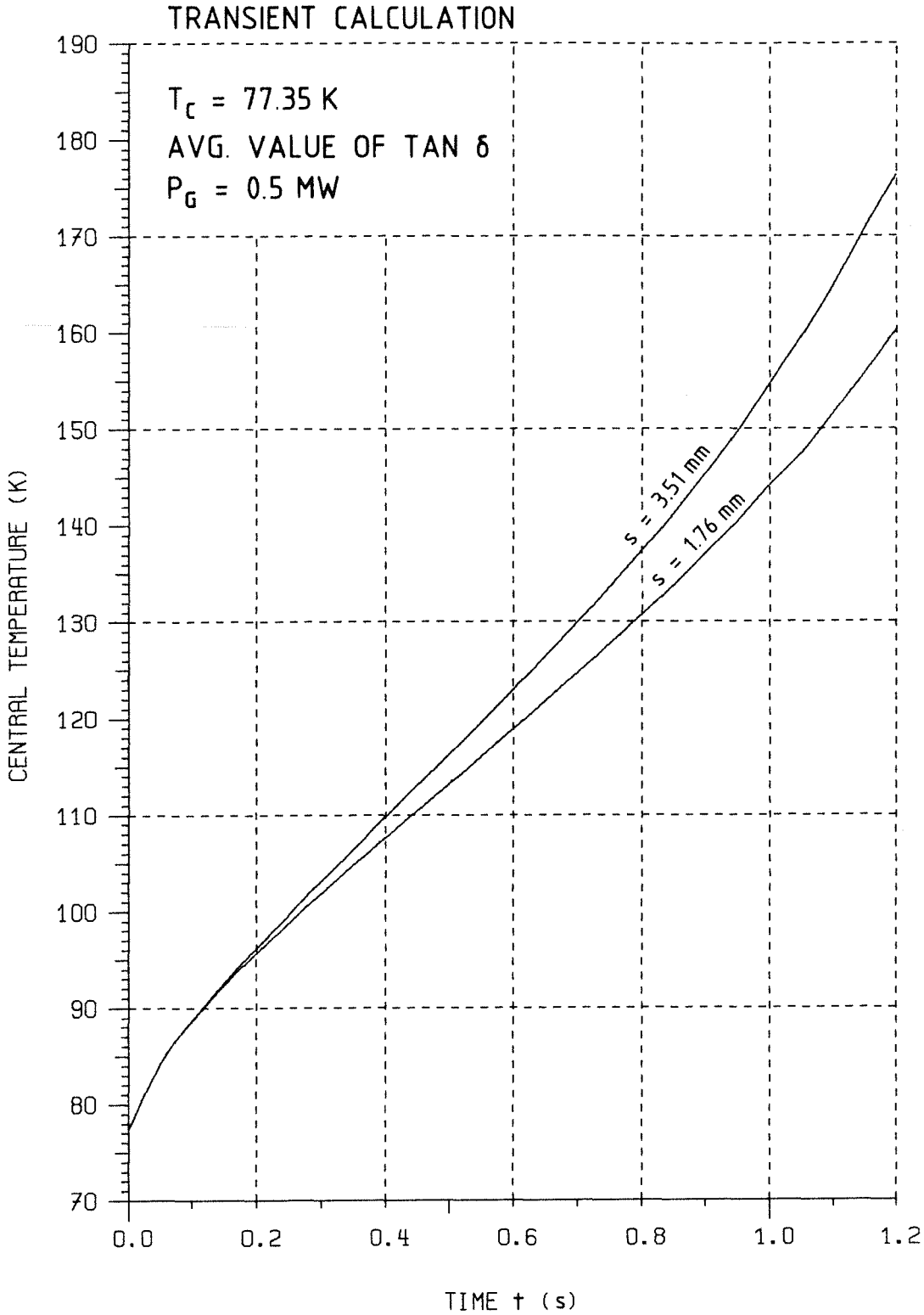

Fig. 36 Development, as a function of time, of the window center temperature vs. the window thickness at P_G = 0.5 MW